https://doi.org/10.5194/egusphere-2024-2263
Preprint. Discussion started: 9 August 2024

The effectiveness of solar radiation management for marine cloud brightening geoengineering by fine sea spray in worldwide different climatic regions

Zhe Song[1*], Ningning Yao[2], Lang Chen[2], Yuhai Sun[2], Boqiong Jiang[2], Pengfei Li[3+], Daniel Rosenfeld[4], Shaocai Yu[2*+]

[1] Research Center for Air Pollution and Health; Key Laboratory of Environmental Remediation and Ecological Health, Ministry of Education, College of Environment and Resource Sciences, Zhejiang University, Hangzhou, Zhejiang 310058, P.R. China
[2] School of Environmental Sciences and Engineering, Zhejiang Gongshang University, Hangzhou 310018, China
[3] State Key Laboratory of Infrared Physics, Shanghai Institute of Technical Physics, Chinese Academy of Sciences, Shanghai 200031, China
[4] Institute of Earth Sciences, The Hebrew University of Jerusalem, Jerusalem, Israel

[*]Equal contribution
[+]*Correspondence to*: Shaocai Yu (shaocaiyu@zjgsu.edu.cn)，Pengfei Li (pengfeili@mail.sitp.ac.cn)

https://doi.org/10.5194/egusphere-2024-2263
Preprint. Discussion started: 9 August 2024

Abstract

Marine Cloud Brightening (MCB) geoengineering aims to inject aerosols over oceans to brighten clouds and reflect more sunlight to offset the impacts of global warming or to achieve localized climate cooling. There is still controversy about the contributions of direct and indirect effects of aerosols in implementing MCB and the lack of quantitative assessments of both. Here, we conducted experiments with injected sea-salt aerosols in the same framework for five open oceans around the globe. Our results show that a uniform injection strategy that did not depend on wind speed captured the sensitive areas of the regions that produced the largest radiative perturbations during the implementation of MCB. When the injection amounts were low, the sea-salt aerosols dominated the shortwave radiation mainly through the indirect effects of brightening clouds, showing obvious spatial heterogeneity. As the indirect effects of aerosols saturated with increasing injection rates, the direct effects still increased linearly and exceeded the indirect effects, producing a consistent increase in the spatial distributions of top-of-atmosphere upward shortwave radiation. Our research emphasizes that MCB was best implemented in areas with extensive cloud cover, while the aerosol direct scattering effects remained dominant when clouds were scarce.

Keywords: marine cloud brightening; solar radiation management; fine sea spray; climatic ocean regions; geoengineering

https://doi.org/10.5194/egusphere-2024-2263
Preprint. Discussion started: 9 August 2024

1. Introduction

As global temperatures continue to rise, the international community is facing an unprecedented challenge to achieve the ambitious goal set in the Paris Agreement of limiting global warming to within 1.5 ^{0}C (Mengel et al., 2018). Even the recent 28th Conference of the Parties (COP28) proposing to phase out all fossil fuels from the current energy system to achieve the global goal on adaptation and its framework, it is also recognized that our current efforts are still insufficient to meet the COP28 goals (https://www.cop28.com/). Against this backdrop, scientists are turning their attentions to more radical and innovative geoengineering methods, attempting to reduce or offset the impacts of climate change through artificial interventions in the climate (Visioni et al., 2023). Some geoengineering methods seek to capture or remove CO_2 from the atmosphere to increase carbon sinks, while others focus on modifying solar radiation, reducing incoming solar shortwave radiation, or reflecting more sunlight to cool the earth, known as solar radiation management (SRM) (Lenton and Vaughan, 2009). Among these, marine cloud brightening (MCB) has a certain realistic basis and is considered the most likely geoengineering method for regional applications (Latham et al., 2014). It has been observed that exhaust emissions from ocean-going vessels can lead to brighter clouds, with clear ship tracks also visible from satellites, and MCB aims to replicate this effect by spraying sea-salt aerosols (Chen et al., 2012).

Aerosol-cloud interactions and their impacts on climate are complex (Rosenfeld et al., 2014, 2019). Injected sea-salt aerosols affect clouds through indirect effects (Paulot et al., 2020). In the case of a constant liquid water content, an increase in cloud droplet number concentration (CDNC) decreases the cloud droplet size, increases the total surface area of cloud droplets, thereby enhancing the cloud albedo, forming brighter clouds, and reflecting more sunlight back (the first indirect effect or Twomey effect) (Twomey, 1974). At the same time, the decrease in cloud droplet size suppresses precipitation, thereby increasing the cloud's lifespan and optical thickness (the second indirect effect of aerosols) (Albrecht, 1989). Reducing the cloud drop size induces a faster evaporation and loss of cloud water. However, the effect of the coarse part of the sea spray aerosols has an opposite effect that offsets the loss of liquid water pass (Liu et al., 2022). In addition, injected aerosols scatter more sunlight back into space through the direct scattering effect (Ahlm et al., 2017; Partanen et al., 2012; Zhao et al., 2021). Therefore, this method is also called marine sky brightening (MSB), which can work even when there are no clouds. Here, we collectively refer to the practice of injecting sea-salt aerosols as MCB. MCB has unique advantages compared to other geoengineering schemes. For example, the sprayed aerosols are non-polluting, and can be applied locally to change the regional climate. Their deployment costs are relatively low and flexible

https://doi.org/10.5194/egusphere-2024-2263
Preprint. Discussion started: 9 August 2024

(Kravitz et al., 2014; Latham et al., 2012, 2014). However, despite these potential advantages, the long-term effects and potential risks of MCB are not fully understood, and there are significant uncertainties as well as ethical, political, and environmental risks. Therefore, most of the current literatures examine the environmental and climate impacts of MCB implementation through modeling.

Table S1 summarized the current modeling experiments on MCB and similar spraying of sea-salt aerosols, as well as their implementation strategies. Most MCB studies used Earth-System Models to assess the impacts of the implementation of MCB on climate. Early MCB studies assumed the effects of MCB implementation by setting a fixed CDNC or directly modifying the cloud effective radius (r_e), ignoring the processes such as generation, transport, dry and wet deposition, and activation of injected sea-salt aerosols, and not including the direct radiative effect of aerosols. With the development of models, researchers started to conduct more detailed studies by injecting aerosols or increasing sea-salt aerosol emissions, taking into account the post-treatment processes of aerosols mentioned above. The implementation region of MCB is crucial, and existing research focused on the impacts of implementing MCB in open oceans globally, the equatorial region (between 30°S and 30°N), and coastal areas with widespread marine stratocumulus clouds. Alterskjær et al. (2012) used the cloud-weighted susceptibility function to find the most sensitive regions to the injection of sea-salt aerosols. Similarly, Jones and Haywood (2012) determined the 10% of the marine regions globally most suitable for implementing MCB through an iterative method. The contributions of direct and indirect effects of aerosols during the implementation of MCB are still controversial and quantitative assessment of both is lacking.

Here, we used the two-way coupled WRF-CMAQ model, combined with previous studies on the region and injection strategies, to implement MCB in five open oceans worldwide. This study simulated the regional radiation and cloud responses caused by injecting sea-salt aerosols. This aims to explore the commonalities and differences in MCB implementation in different regions and to seek the optimal strategy for MCB injection.

2. Experiments and methods

2.1 Model configuration

The two-way coupled Weather Research and Forecasting (WRF v3.4) - Community Multi-scale Air Quality (CMAQ v5.0.2) model that considered both direct and indirect effects of aerosols was used in this study[43]. In the two-way coupled model, aerosols predicted by CMAQ were able to affect clouds, radiation, and precipitation simulated by WRF in a consistent online coupled manner (Wong et al., 2012).

https://doi.org/10.5194/egusphere-2024-2263
Preprint. Discussion started: 9 August 2024

Yu et al. (2014) further extended the two-way coupled WRF-CMAQ model by incorporating the aerosol indirect effects (including the first, second, and glaciation aerosol indirect effects), improving the ability of the WRF-CMAQ model to predict clouds and radiation. Wang et al. (2021) validated this model.

The physical schemes of the WRF model are the same as those set in Yu et al. (2014), including the asymmetric convective model (ACM2) for a planetary boundary layer (PBL) scheme (Pleim, 2007), the Morrison 2-moment cloud microphysics scheme (Morrison et al., 2009), the Kain-Fritsch (KF2) cumulus cloud parameterization, the Rapid Radiative Transfer Model for General Circulation Models (RRTMG) longwave and shortwave radiation schemes, and the Pleim-Xiu (PX) land-surface scheme. The meteorological initial and boundary conditions were provided by the National Center for Environmental Prediction (NCEP) final analysis dataset (FNL) with a spatial resolution of 1°×1° and temporal resolution of 6 h. The carbon bond gas-phase chemical mechanism (CB05) and aerosol module of AERO6 were used in the CMAQ model. The anthropogenic emissions were taken from the Hemispheric Transport of Air Pollution (HTAP_V2) projects (Janssens-Maenhout et al., 2015). The biogenic emissions were estimated by the Biogenic Emissions Inventory System version 3.14 (BEISv3.14) model (Carlton and Baker, 2011). Sea salt emissions were calculated online in CMAQ and were divided into open-ocean and surf-zone emissions. In the open ocean, Gong (2003) extended the sea-salt aerosol parameterization of Monahan et al. (1986) to submicron sizes, with the emission flux being linearly proportional to the ocean area covered by whitecaps. The geometric mean diameter of accumulation mode sea-salt aerosols in the CMAQ ranged from 0.2651 to 0.8187 μm. The particle size distributions of the emitted sea-salt aerosols were adjusted to the local relative humidity before mixing with the ambient particle modes (Zhang et al., 2005). Surf-zone emissions were calculated using the open ocean-source function of Gong (2003), with a fixed whitecap coverage of 100% and a surf-zone width of 50 m. Kelly et al. (2010) provided a detailed description of these processes. In the CMAQ model, the number concentration emission rate was calculated from the mass emissions rate as follows:

$$E_{3n} = \left(\frac{6}{\pi}\right)\left(\frac{E_n}{\rho_n}\right) \tag{1}$$

$$E_0 = \frac{\sum_n E_{3n}}{D_{\mathrm{gv}}^3 \exp\left(-\frac{9}{2}\ln^2 \sigma_{\mathrm{g}}\right)} \tag{2}$$

where En was the mass emissions rate for species n and ρ_n was the density for that species. The sum $\sum_n E_{3n}$ was taken over all emitted species. The geometric mean diameter for mass or volume, D_{gv}, was given by $D_{gv} = D_g \exp(3 \ln^2\sigma_g)$ from the Hatch-Choate relations for a lognormal distribution (Binkowski

https://doi.org/10.5194/egusphere-2024-2263
Preprint. Discussion started: 9 August 2024

and Roselle, 2003). This study used Geographic Information System software (ArcGIS) to obtain the open-ocean and surf-zone fractions for each grid within the modeling domain from shoreline information. The modeling domains of the five regions were almost entirely open ocean, with surf-zone fractions of less than 0.01%.

2.2 Experimental setup

As summarized in Table S1, the MCB geoengineering implementation areas included the globe, the equator (30°S–30°N), regions with extensive coverages of marine stratocumulus clouds, and so on. Therefore, based on previous experimental designs, we used the WRF-CMAQ model to simulate the injections of sea-salt aerosols in the five open ocean regions (Fig. 1c). These regions were Asia, located in East Asia on the western side of the Pacific Ocean; Equa, situated in the Philippine Sea along the equator; and NP, SP, and SA, which referred to the North Pacific, South Pacific, and South Atlantic, respectively. These three regions, located along the western coast of continents, were considered to have extensive coverage of marine stratocumulus clouds and were the most suitable areas for implementing MCB (Alterskjær et al., 2012; Hill and Ming, 2012; Jones et al., 2009; Partanen et al., 2012; Stuart et al., 2013). The grid numbers of WRF and CMAQ were 190×190 and 173×173, respectively, and both had a horizontal resolution of 12 km, with 29 vertical layers from the surface to about 21 km altitude. The simulation period for the Asia, Equa, and NP regions in the northern hemisphere was from July 24, 2018, to September 1, 2018, while for the SP and SA regions in the southern hemisphere, the simulation period was from February 24, 2023, to April 1, 2023. The first 8 days of the model simulations were considered as the spin-up period to minimize the impacts of initial chemical conditions.

We tested four different sea-salt aerosol injection methods, wind-speed-dependent **Natural×5**, **Wind-adjusted**, **Fixed-wind-adjusted** and **Fixed-wind-adjusted** uniform injections of sea-salt aerosols at a fixed rate of 10^{-9} kg m^{-2} s^{-1}. All additional injected sea-salt aerosols were in the accumulation mode. In this study, the geometrical mean dry diameter of sea-salt aerosols injected into the five regions was about 0.11–0.15 µm, and was similar for all emission scenarios.

Natural×5: Increased the emission rates of accumulation mode sea-salt aerosols by a factor of 5 (Hill and Ming, 2012). This was a simple wind-speed-dependent increase. The injection rates in the five regions were equivalent to 0.03–0.09×10^{-9} kg m^{-2} s^{-1} (Table S2).

Wind-adjusted: Salter et al. (2008) designed a spray vessel for injecting sea-salt aerosols with a spray efficiency that was dependent on wind speed and was expected to achieve maximum spray outputs

https://doi.org/10.5194/egusphere-2024-2263
Preprint. Discussion started: 9 August 2024

at wind speeds between 6–8 m s^{-1}. The threshold wind speed was set to 7 m s^{-1} and the spray efficiency at lower wind speeds was 1.5 times the wind speed. We used the source function of Partanen et al. (2012) as follows, where u was the 10 m wind speed. For example, at wind of 7 m s^{-1} the injection rate would be 0.26 × 10^{-9} kg m^{-2} s^{-1}.

$$F_{\mathrm{m,\,baseline}} = \begin{cases} 5 \times 2.8 \times 10^{-12} \times \left(\frac{u}{1\ \mathrm{m\,s^{-1}}}\right)^{1.5} \mathrm{kg\,m^{-2}s^{-1}}, & u < 7\ \mathrm{m\,s^{-1}} \\ 5 \times 2.8 \times 10^{-12} \times 7^{1.5}\ \mathrm{kg\,m^{-2}s^{-1}}, & u \geq 7\ \mathrm{m\,s^{-1}} \end{cases} \quad (3)$$

Fixed at 10^{-9} kg m^{-2} s^{-1}: Unlike the previous two injection methods, the injections of sea-salt aerosols at a fixed rate of 10^{-9} kg m^{-2} s^{-1} were not dependent on wind speed and increased uniformly over all ocean grids. Injecting sea-salt aerosols at a fixed rate identified the geographic areas that were most sensitive to increased sea-salt aerosols and produced the largest top-of-atmosphere (TOA) radiative perturbations (Alterskjær et al., 2012). Many other studies have used this method (Goddard et al., 2022; Horowitz et al., 2020; Mahfouz et al., 2023).

Fixed-wind-adjusted: To rule out differences in radiative and cloud response due to wind variabilities on spray rates, we performed an additional adjustment. Similar to **Natural×5**, the injections of sea-salt aerosols were also dependent on the wind speed but the integrated amounts in the region were set to be equal to the case that all area had a fixed rate of **10^{-9} kg m^{-2} s^{-1}** (**Fixed**).

2.3 Calculations

The calculation method related to radiation, cloud properties, and cloud radiation forcing was based on Goddard et al. (2022), briefly described here as follows. This study focused on the shortwave radiative flux responses at the TOA due to the injections of sea-salt aerosols, which was consistent with the definition of effective radiation forcing (ERF) (Forster et al., 2007). The sea surface temperature in the model was preset by NCEP-FNL, so the model's surface temperature and upward longwave radiation would not respond to the increased sea-salt aerosols. The total upward shortwave radiation flux (SW_TOT) at the TOA was under the all-sky conditions. The responses of SW_TOT to the injections of sea-salt aerosols could be divided into the cloud radiation effects (SW_CLD, excluding the influence of aerosols) and the direct scattering effects when clouds were present (SW_AER).

$$\mathrm{SW\_TOT} = \mathrm{SW\_CLD} + \mathrm{SW\_AER} \quad (4)$$

The diagnosis of CLEAN-SKY (no aerosols) was not considered in the previous WRF-CMAQ model. So in this study, we extended this feature in the WRF-CMAQ model using the methodology of Ghan et al. (2012) by performing a double radiative call at each time step to calculate radiation variables related

https://doi.org/10.5194/egusphere-2024-2263
Preprint. Discussion started: 9 August 2024

to CLEAN-SKY (SW_CLD). We have also studied the impacts of injecting sea-salt aerosols on the upward shortwave radiation flux at the TOA under the clear-sky conditions (SW_AER_CLR). At this time, only the direct scattering effect of aerosols existed, which was considered to be the maximum MSB potential generated by injecting sea-salt aerosols when there were no clouds. Unless otherwise specified, all results in this study were monthly averages.

Due to the different amounts of sea-salt aerosols injected in different ways, it resulted in different SW_TOT responses. Therefore, we proposed the concept of MCB efficiency (E_{MCB}) to measure the relationships between the amount of sea-salt aerosol injections and the resulting radiation flux responses.

$$E_{MCB} = \frac{\text{SW\_TOT response due to injection of sea-salt aerosol (W m}^{-2}\text{)}}{\text{Sea-salt aerosol injections (kg } m^{-2}\, s^{-1}\text{)}} \quad (5)$$

It measured the efficiency of implementing MCB in different regions, that was, how much SW_TOT responses were expected to be generated by injecting sea-salt aerosols at a rate of 1 kg m^{-2} s^{-1}. E_{MCB} = 1 means that injecting 1 kg of sea-salt aerosols per unit time in the current study area was expected to produce a 1 GW (10^9 W) SW_TOT response. Note that this value (E_{MCB}) was based on model calculations under specific atmospheric conditions within the study region and was only used to analyze the sensitivities of the radiative flux to different injection methods and injection amounts.

This study focused on the changes in liquid clouds and evaluated the responses in cloud condensation nuclei (CCN), cloud fraction, CDNC, r_e, liquid water path (LWP), cloud optical thickness (COT), and cloud albedo due to the injections of sea-salt aerosols. These calculations were shown in Supplementary Text S1.

Cloud radiation forcing (CRF) parameters can be used to quantify the responses of SW_CLD to changes in cloud cover or cloud albedo, defined as follows (Goddard et al., 2022):

$$\text{CRF}_{param} = \alpha_c f \quad (6)$$

where α_c was mean cloud albedo and f was mean cloud fraction.

The CRF parameters could be approximated using the perturbation method as follows (Goddard et al., 2022):

$$\text{CRF}'_{param} = \alpha'_c \bar{f} + \bar{\alpha}_c f' + \alpha'_c f' \quad (7)$$

where the first term on the right-hand side indicated the changes in CRF_{param} driven by the perturbation of cloud albedo, the second term indicated the changes driven by the perturbation of cloud fraction, and the third term denoted the changes driven by the interactions of the two. The horizontal bars on α_c and f were defined as the monthly means of the Base, and the prime (') defined the monthly mean differences

https://doi.org/10.5194/egusphere-2024-2263
Preprint. Discussion started: 9 August 2024

between the sensitivity experiments and Base. The fourth column of Fig. S24 shows that the differences between CRF_{param} and CRF'_{param} were small enough that the perturbation method could be used to approximate the CRF'_{param}.

The changes in cloud albedo were driven by multiple processes. Based on Quaas et al. (2008) and Christensen et al. (2020), Goddard et al. (2022) established the following equation to assess the relative effects of CDNC, LWP, and mean cloud fraction on the responses of SW_CLD due to the injections of sea-salt aerosols:

$$\frac{\Delta\alpha}{\Delta \ln \mathrm{AOD}} = f\Delta\alpha_c(1-\alpha_c)\left(\frac{1}{3}\frac{\Delta \ln \mathrm{CDNC}}{\Delta \ln \mathrm{AOD}} + \frac{5}{6}\frac{\Delta \ln \mathrm{CLWP}}{\Delta \ln \mathrm{AOD}} + \frac{\Delta \ln f}{\Delta \ln \mathrm{AOD}}\right) \quad (8)$$

where α was the planetary albedo, Δ represented the difference in monthly average results between sensitivity experiments and Base simulations, and α_c was the cloud albedo. The three terms inside the right parenthesis represented the relative contributions of Twomey effect, LWP effect, and cloud fraction effect, respectively, with the latter two related to the second aerosol indirect effect (Albrecht, 1989).

3. Results

3.1 The impacts of different injection strategies on shortwave radiation at the TOA.

In modeling studies, using different methods to increase sea-salt aerosols may lead to different conclusions, and this discrepancy may be one of the reasons for differences in the assessments of MCB potentials in previous studies. In this study, sea-salt aerosols injected in different strategies (with dry diameters of about 0.11–0.15 μm, Fig. 1a) increased the SW_TOT at the TOA by 0.06–24.50 W m^{-2} in the five ocean regions (Fig. 2). The Natural×5 and Wind-adjusted methods, which relies on wind speeds, injected sea-salt aerosols of 0.03–0.09 and 0.18–0.21 $\times 10^{-9}$ kg m^{-2} s^{-1} into the five regions, respectively, resulting in SW_TOT variations of 0.06–2.08 and 1.35–8.47 W m^{-2} (Table S2), respectively. Except for the Equa region, the other four regions can initially achieve the radiation flux responses required to offset the radiative forcing of 3.7 W m^{-2} due to doubling of atmospheric CO_2 concentration since industrialization (Latham et al., 2008; Ramaswamy et al., 2001). Uniformly injections of sea-salt aerosols at a fixed rate of 10^{-9} kg m^{-2} s^{-1} resulted in SW_TOT changes of 10.96–24.50 W m^{-2} in the five regions. This value far exceeded the radiation flux response envisioned for offsetting geoengineering, so we only used it to explore the sensitivities of different injection methods and regional responses, and subsequent studies on the impacts of injecting sea-salt aerosols in sensitive areas on the entire region. The three continental west coast stratocumulus regions of NP, SP, and SA had the most significant SW_TOT responses, all exceeding 20 W m^{-2}, while the SW_TOT responses in the Asia and Equa regions were 17.34

https://doi.org/10.5194/egusphere-2024-2263
Preprint. Discussion started: 9 August 2024

and 10.96 W m^{-2}, respectively.

Injecting the same amount of sea-salt aerosols resulted in substantial variations in SW_TOT responses across the different regions (Fig. S1). The sea-salt aerosols sprayed in the Fixed-wind-adjusted experiments were also dependent on wind speed, but the amount of emission rate integrated in the full domain was consistent with the fixed rate of 10^{-9} kg m^{-2} s^{-1}, ruling out the differences caused by the amount of injected sea-salt aerosols. Although both methods injected the same amounts of sea-salt aerosols, the SW_TOT responses they produced were significantly different. The Fixed-wind-adjusted method resulted in SW_TOT changes of 5.00–19.78 W m^{-2} in the five regions, indicating that the shortwave radiation flux changes caused by wind-speed-dependent injections were smaller than those caused by uniformly injections, and showed regional differences. Due to the different amounts of sea-salt aerosol injected in different ways, it resulted in different SW_TOT responses. Therefore, we proposed the concept of MCB efficiency (E_{MCB}) to measure the relationships between the amounts of sea-salt aerosol injections and the resulting radiation flux responses. E_{MCB} = 1 GW kg^{-1} s means that injecting 1 kg of sea-salt aerosols per unit time in the current study area was expected to produce a 1 GW (10^9 W) SW_TOT response. Figure 3 shows the E_{MCB} values of different sea-salt injection strategies in the five regions. Overall, MCB implementation was more efficient in the NP, SP, and SA regions, while it was less efficient in the Asia and Equa, which was similar to the previous SW_TOT response results. E_{MCB} also varied for different injection methods. In the NP, SP, and SA regions, the E_{MCB} values of the Natural×5 and Wind-adjusted methods with relatively small injection amounts were higher. With the increases in sea-salt aerosols injections, E_{MCB} decreased (discussed below). At the same injection amount, injecting at a fixed rate shows higher E_{MCB} compared to injections dependent on wind speed, as consistently shown in all five regions.

The productions of sea-salt aerosols in nature were strongly correlated with wind speed, and most models associated sea-salt aerosol emissions with wind speed (Ahlm et al., 2017; Grythe et al., 2014). Injection strategies depending on wind speed made the distributions of added sea-salt aerosols closer to the natural distributions. In natural environments, sea-salt aerosol emissions in strong-wind areas (e.g., storm or typhoon areas) and surf zones are usually much larger than in weak-wind areas. Therefore, injection methods depending on wind speed concentrated the added sea-salt aerosols in strong-wind areas and surf zones, while the weak-wind regions increased relatively little sea-salt aerosols (Fig. S2). Injecting uniformly at a fixed rate in the model would result in a large increase of sea-salt aerosols in places with originally low aerosol concentrations (e.g., weak-wind regions). Therefore, when using models to

https://doi.org/10.5194/egusphere-2024-2263
Preprint. Discussion started: 9 August 2024

simulate the injections of sea-salt aerosols by increasing the emission rate, it was necessary to consider the impacts of different injection methods on the distributions of sea-salt emissions. Using a uniformly increasing method independent of wind speed can not only avoid the situation of a smaller increase in sea-salt emissions in regions with lower wind speeds, but can also identify the geographical areas most sensitive to the increased sea-salt aerosols and producing the largest TOA radiation perturbations (Alterskjær et al., 2012).

Uniform injections of sea-salt aerosols throughout the region ignored the transport and diffusion of aerosols. Therefore, we captured the geographical areas with the most sensitive and largest TOA radiation disturbances due to uniform injections in various ocean regions (30 × 50 grids, approximately 360 km × 600 km, and away from the domain boundaries). Injecting sea-salt aerosols in the sensitive areas with the same uniform injections (10^{-9} kg m^{-2} s^{-1}, the injection rate is about 1/20 of the full domain injection) resulted in changes of 0.65–3.27 W m^{-2} in SW_TOT in the five ocean regions (Table S2). The SW_TOT responses were the largest in the SP region, at 3.27 W m^{-2}, and 2.69 and 1.81 W m^{-2} in the NP and SA regions, respectively, while they were only 0.65 and 0.74 W m^{-2} in the Asia and Equa regions, respectively. The injected sea-salt aerosols produced SW_TOT changes of 5.14–15.22 W m^{-2} in the sensitive areas (Fig. 1b). Similarly, the increases in SW_TOT in the SP, SA, and NP regions all exceeded 10 W m^{-2}, with the highest in the SP region at 15.22 W m^{-2}. In the Asia and Equa regions, although the increases in SW_TOT were only 6.22 and 5.14 W m^{-2}, respectively, it can still achieve the goal of offsetting the overall effective radiative forcing produced by anthropogenic activities in the sensitive areas. Also, when injecting at a uniform rate of 10^{-9} kg m^{-2} s^{-1} within the sensitive areas, for the entire region, the MCB efficiencies were greatly improved for all sea areas except Asia (Fig. S3). Considering that the original intents of MCB or MSB design were regional application (hurricane mitigation, coral reef protection and polar sea ice recovery), choosing to inject sea-salt aerosols in the sensitive areas could achieve the corresponding cooling goals within the region, and also affected larger areas through the diffusions and transports of aerosols.

3.2 Characterization of the radiation responses.

SW_TOT responses were defined as the sum of the upward shortwave radiation flux response at the TOA generated by the combined effects of the direct scattering effect of aerosols (SW_AER) and cloud radiative effect (SW_CLD) after injecting sea-salt aerosols. Figure 4 shows the contributions of SW_AER and SW_CLD responses in the SW_TOT produced by different injection methods in the five ocean

https://doi.org/10.5194/egusphere-2024-2263
Preprint. Discussion started: 9 August 2024

regions. The majority of the SW_TOT radiative flux response due to the less injected Natural×5 and Wind-adjusted strategies was caused by the SW_CLD response (Fig. 4 and Table 1). In the NP, SP, and SA regions, the contribution of SW_CLD exceeded 70%, suggesting that sea-salt aerosols injected at these locations increased the SW_TOT mainly by affecting clouds through indirect effects. In the Equa, the responses of SW_TOT were entirely caused by SW_AER. The proportion of SW_AER produced by the uniform injection of sea-salt aerosols at a fixed rate of 10^{-9} kg m^{-2} s^{-1} continued to increase (Fig. 4c). In the Asia, Equa, and SP regions, the proportion of SW_AER exceeded that of SW_CLD. In the SA region, SW_CLD and SW_AER were almost equal, while in the NP region, the SW_CLD response was 13.41 W m^{-2}, still greater than SW_AER (9.70 W m^{-2}). This is because there was a saturation phenomenon in the cloud response to aerosols injections (discussed below), and the NP, SP, and SA regions provided more SW_CLD responses, while the cloud responses in the Asia and Equa regions saturated and no longer increased. The results of Fixed-wind-adjusted case show that, at the same injection amount, the SW_AER responses caused by the injection method relying on wind speed was significantly smaller than those of the method with fixed-rate uniform injection, while the disparity in SW_CLD responses was minimal. This is because the injection method relying on wind speed distributed most of the increased sea-salt aerosols to areas with already high emissions, such as strong-wind areas and surf zones, where the excess marine aerosols had already saturated the cloud responses, resulting in minor changes in SW_CLD. In areas with weak winds, the potentials for direct aerosol scattering were not fully exploited due to the relatively small amounts of sea-salt aerosols injected, leading to a lower SW_AER response.

Figures S4 and S5 show the spatial distributions of SW_CLD and SW_AER responses resulting from different injection methods in the five ocean regions. The SW_CLD responses were stronger in the three regions of NP, SP, and SA, while they were weaker in the regions of Asia and Equa, and in some grids they even led to a reduction of the upward shortwave radiation. The spatial distributions of the SW_CLD responses exhibited noticeable discontinuity, reflecting significant regional differences in the non-uniform distributions of clouds and their impacts on shortwave radiation at the TOA. Due to the influences of various complex factors on cloud formations and distributions, simulation results related to clouds show significant spatial variabilities. This might be the result of the combined effects of local meteorological conditions and changes in cloud physical properties caused by sea-salt aerosol injections.

In contrast, the spatial distributions of the SW_AER response were smoother, leading to consistent increases in upward shortwave radiation at the TOA in all ocean regions. This indicates smaller spatial limitations in the distributions of aerosol particles, allowing direct scattering effects to take place

https://doi.org/10.5194/egusphere-2024-2263
Preprint. Discussion started: 9 August 2024

everywhere. The direct scattering effect of aerosols was primarily related to the concentrations and physical properties of the particles (discussed below), unlike clouds, which were influenced by multiple variables. These results suggest that when implementing geoengineering measures, it is essential to comprehensively consider the interactions between aerosols and clouds, as well as their different response patterns in various regions. Furthermore, the high spatial variabilities of cloud radiation effects emphasized the need for improved resolution in future model studies of cloud-aerosol interactions.

The SW_CLD response resulting from the injection of sea-salt aerosols in the sensitive areas of five ocean regions exhibits significant spatial differences. The SW_CLD response is larger than the SW_AER response in the sensitive areas of NP, SP, and SA, indicating that the changes in SW_TOT are mainly driven by the cloud radiation response (Fig. 5). In contrast, the SW_CLD response is smaller in the Asia and Equa regions. This regional difference is similar to that observed with uniform injection across the entire region. The SW_AER response shows consistent results in all areas, resulting in a radiation response change of 3.55–5.42 W m^{-2} within the injection areas. In the Asia and Equa, the variations in SW_TOT were primarily driven by the direct scattering effects of aerosols.

Aerosols can have a greater impact on radiation responses outside the sensitive areas through transports and diffusions, reaching up to three times the total radiation within the sensitive areas (Fig. 6). In all regions except Asia, the total SW_CLD response outside the sensitive region was about 270%–408% higher than inside. In Asia, the SW_CLD response outside the sensitive area was only 29% of the response inside. The SW_CLD responses in NP, SP, and SA extended to the west and northwest of the injection areas, indicating that clouds in these areas were affected by the injection of sea-salt aerosols (Fig. 5). Changes in cloud microphysical properties would be presented later. The SW_CLD variations in other directions were not uniform, and there was negative SW_CLD responses in some grids, which again reflected the spatial complexities of cloud radiation effects. The direct scattering effects of aerosols on areas outside the sensitive region is reflected in a widespread increase in upward shortwave radiation at the TOA. The total SW_AER responses outside the sensitive areas in the five ocean regions were approximately 160%–281% higher than inside, but lower than the impacts of SW_CLD responses outside the sensitive areas. There were consistencies in the spatial distributions of SW_AER and SW_CLD responses.

3.3 Saturation of the cloud radiative responses.

Figure 7 shows that under low levels of sea-salt aerosol injections, radiation response changes were

https://doi.org/10.5194/egusphere-2024-2263
Preprint. Discussion started: 9 August 2024

mainly driven by SW_CLD responses. As the injected sea-salt aerosols increased, the SW_CLD responses gradually reached saturation. After reaching a certain injection level, the increases of SW_CLD responses stabilized at its maximum value and no longer increases with further injections. The SW_CLD responses show large differences in the five ocean regions, and the different shapes and slopes of the curves indicated that the cloud radiative forcing responses to the sea-salt aerosol injections were different in each region. This might be due to variations in cloud types, cloud amounts, and atmospheric conditions in the different regions. In the NP, SP, and SA, the SW_CLD responses exceeded 10 W m^{-2}, while in Asia, it saturated at 5 W m^{-2}. In Equa, when the sea-salt aerosol injection rate was 10^{-9} kg m^{-2} s^{-1}, the SW_CLD response was 0.54 W m^{-2}, and even when the injection doubled, the SW_CLD response remained at 0.54 W m^{-2}. This implies that the SW_TOT at Equa was almost exclusively from the contributions of the direct scattering effects of aerosols.

In contrast to SW_CLD, the SW_AER responses increased linearly with the injections of sea-salt aerosols ($R^2 > 0.99$). As the injection increased, the contributions of SW_AER to SW_TOT gradually increased, surpassing the SW_CLD responses, and showed the same trends across the five regions. This implies that at higher injection levels, the contributions of SW_CLD to total radiation change saturated, and cloud properties no longer significantly changed. At this point, sea-salt aerosols primarily affected radiation through direct scattering effects, and the aerosol particles' ability to scatter solar radiation continued to increase with the increases in aerosol quantities. In some cloud-free regions or weather conditions, injected sea-salt aerosols were still able to function through direct scattering.

There existed a specific injection level at which the SW_CLD and SW_AER responses were equal. In the NP region, when the injection level was approximately 1.55×10^{-9} kg m^{-2} s^{-1}, both SW_CLD and SW_AER responses were 15 W m^{-2}. In the SP and SA, these levels were about 0.67×10^{-9} kg m^{-2} s^{-1} and 1×10^{-9} kg m^{-2} s^{-1}, respectively. While in Asia, the responses were already equal when the injection amount was 0.15×10^{-9} kg m^{-2} s^{-1}. Since there was a saturation of the cloud radiation effects, E_{MCB} decreased with the increases in sea-salt aerosol injection amounts (Fig. 7, red dashed line). This can also explain the higher E_{MCB} of the Natural×5 and Wind-adjusted methods with relatively low injection amounts (Fig. 3). When less sea-salt aerosols were injected, both SW_CLD and SW_AER responses contributed to the changes of SW_TOT. As the injection amounts increased, the SW_CLD responses saturated, and the increases in SW_TOT depended on the increases in SW_AER responses, leading to a decrease in E_{MCB}. Therefore, implementing geoengineering with sea-salt aerosol injections required considering local atmospheric conditions and balancing the relationships between cooling goals and sea-salt injection

https://doi.org/10.5194/egusphere-2024-2263
Preprint. Discussion started: 9 August 2024

efficiencies.

Under clear and cloudless conditions, injecting sea-salt aerosols could still increase the SW_TOT through direct scattering, and this effect exceeded those of aerosol direct scattering when clouds were present. The variations of the upward shortwave radiation flux at the TOA under the clear-sky conditions (SW_AER_CLR) did not exhibit significant regional heterogeneity across the ocean areas (Figs. 5 and S6), suggesting that the contribution of direct aerosol scattering was more uniform globally when considering the effects of sea salt injections on the Earth's radiation budget. The SW_AER_CLR responses were also linearly correlated with the injection of sea-salt aerosols ($R^2 > 0.99$), and it exceeded the SW_AER responses (Fig. 7). This is because cloud layers also scattered and absorbed solar radiation, so this scattering effect was more significant under clear sky conditions. It was reflected that in regions with strong cloud radiation effects, such as the NP, SP, and SA regions, the differences between the SW_AER and SW_AER_CLR responses were also larger (Fig .7). When injecting sea-salt aerosol in sensitive areas, the spatial distributions of SW_AER_CLR and SW_AER responses were highly consistent (Fig. 5). Therefore, injecting sea-salt aerosol under conditions of low cloud covers or clear skies also increased the upward shortwave radiation flux at the TOA.

3.4 Factors affecting the radiation effects.

The direct radiative effect of aerosols is mainly determined by their own optical properties. In WRF-CMAQ, the emitted sea-salt aerosol particle size distributions were adjusted to the local relative humidity (Kelly et al., 2010; Zhang et al., 2005). The dry diameter of sea-salt aerosols injected into the five regions was about 0.11–0.15 µm (Figs. 1a and S7), and the wet diameter was about 0.22–0.3 µm (Fig. S8). The single scattering albedo (SSA) of aerosols describes the ratio of aerosol particles' ability to absorb and scatter solar radiations. After the injection of sea-salt aerosols, the SSA of the accumulation mode aerosols in the five regions generally increased by about 0.003–0.005, and in some regions within the area, the SSA increased by over 0.007, with an average increase of 0.001–0.003 in sensitive areas (Fig. S9). This indicates that the injected sea-salt aerosol particles could scatter sunlight more effectively than absorb it, causing solar radiation to be reflected back into space. The asymmetry factor of aerosols is a parameter describing the directionality of aerosol particle scattering of sunlight, and an important factor for evaluating direct aerosol radiative forcing (Zhao et al., 2018). The injection of sea-salt aerosols in the five regions reduced the asymmetry factor by 0.007–0.029, with an average reduction of 0.01–0.027 in sensitive areas (Fig. S10). This indicates that the injected sea-salt aerosols tended to scatter more

https://doi.org/10.5194/egusphere-2024-2263
Preprint. Discussion started: 9 August 2024

uniformly or backward rather than in a forward direction.

Uniform injections of 10^{-9} kg m^{-2} s^{-1} sea-salt aerosols led to an increase in aerosol optical depth (AOD) of 0.2–0.37 in all regions (Fig. 8). The distributions of AOD within the regions were not uniform due to aerosol transports and diffusions, with some areas showing an increase in AOD of over 0.6. Injecting sea-salt aerosols in sensitive areas led to an AOD increase of 0.08–0.12, while outside the injection areas, AOD gradually decreased as the aerosols were transported and dispersed. With the increases in sea-salt aerosol injections, AOD showed a linear increase within a certain range in all five ocean regions ($R^2 > 0.997$, Fig. 9a). There was a strong correlation between the AOD changes caused by sea-salt injection and the SW_AER responses. When sea-salt aerosols were uniformly injected across the entire region, the correlation coefficients between AOD and SW_AER responses in the five ocean areas were greater than 0.94, and when injected in sensitive areas, the correlation coefficients were greater than 0.99 (Fig. S11). There was also a strong spatial consistency between the spatial distribution of AOD and SW_AER response (Fig. S5, third row, and Fig. 8, second column; Fig. 5, second column, and Fig. 8, third column).

There were significant differences in the distributions of clouds in the five ocean regions during the study period, with wide distributions of liquid clouds in the NP, SP and SA regions, and less clouds in Asia and Equa. The cloud heights were distributed between 500–2000 meters, centered around 1000 meters (Figs. S12 and S14). In the regions with higher cloud cover, such as NP, SP, and SA, injected sea-salt aerosols significantly increased cloud fraction, leading to the formations of more clouds or expanding the coverage, vertical thickness and lifetime of existing clouds (Goddard et al., 2022).The injection of sea-salt aerosols in sensitive areas had similar results, where cloud fractions increased both inside the injection areas and in the regions affected by aerosol transports and diffusions (Fig. S13).

The injected sea-salt aerosols affected the cloud microphysical properties through indirect effects, thereby influencing cloud radiative responses. Taking the SP region as an example, Fig. 10 demonstrates that uniformly injections of 10^{-9} kg m^{-2} s^{-1} sea-salt aerosols significantly increased the CDNC. More cloud droplets captured more water vapor, leading to an increase in liquid water path (LWP). Additionally, the increases in cloud thickness also contributed to the increase in LWP. The increases in CDNC decreased the mean r_e by 8.9 μm (~ -37%), increased the cloud optical thickness (COT) by more than 220%, and ultimately increased the mean cloud albedo over the region by 0.19 (~64%). Similarly, injecting sea-salt aerosols in the NP and SA regions led to average cloud albedo increases of 0.17 and 0.20, respectively, while in the Asia and Equa, the increases were 0.15 and 0.13, respectively (Figs. S15–S18). The injections

https://doi.org/10.5194/egusphere-2024-2263
Preprint. Discussion started: 9 August 2024

of sea-salt aerosols within the sensitive areas had less effect on cloud microphysical properties than the whole region injections. This is because when sea-salt aerosols were injected across the entire region, the surrounding sea-salt aerosols affected the sensitive areas through transports, resulting in an enhanced cumulative effect on cloud microphysical properties in the sensitive areas. Injecting sea-salt aerosol in the sensitive area of the SP affected clouds in the surrounding region through transports, increased the average cloud albedo across the entire area by 0.03 over the entire region and by 0.12 within the sensitive regions, which was less than the effects of injection across the entire area (Fig. S19). Similarly, injecting sea-salt aerosols in the sensitive areas of other sea regions led to average cloud albedo increases of 0.01–0.02 across the entire area, with increases of 0.11 in the sensitive areas of the SP and SA regions, and increases of 0.09 and 0.10 in the Asia and Equa, respectively (Figs. S20–S23).

3.5 Drivers of SW_CLD responses.

The cloud radiation forcing (CRF) parameters were used to calculate the effects of changes in cloud cover and cloud albedo on the SW_CLD responses due to the injections of sea-salt aerosols. Figure S24 illustrates the increase in the CRF parameter coinciding with the increases in the SW_CLD responses after uniform injection of sea-salt aerosols in the five regions (Fig. S4, third row). The results were similar for injections in the sensitive areas (Fig. S25, third column, and Fig. 5, first column). The CRF'_{param} calculated using the perturbation method indicates that in the five ocean regions, CRF'_{param} was primarily driven by perturbations in cloud albedo (Fig. S26, first column), and it significantly surpassed the changes in cloud fractions and their interactions. Cloud albedo changes explained over 70% of the CRF'_{param} in all four regions except the Equa. The contributions of cloud fraction changes ranged from 13.9% to 23.8%, while the interactions between the two factors accounted for only about 10% (Fig. S26, second and third columns). The results were similar for injections in sensitive regions, where changes in cloud albedo accounted for 68.9%–79.6% of the CRF'_{param}, followed by changes in cloud fractions, with the smallest contributions from their interactions (Fig. S27).

Figure 11 evaluates the relative effects of Twomey, LWP, and cloud fractions on the SW_CLD responses after uniformly injecting sea-salt aerosols in five ocean regions. The results indicate that changes in CDNC (Twomey effect) and LWP were the main drivers of SW_CLD responses, while changes in cloud fraction contributed minimally to the SW_CLD responses. Except for the Equa region, changes in CDNC and LWP accounted for 48.2%–52.4% and 38.9%–41.9% of the SW_CLD changes, respectively, with cloud fraction changes contributing to less than 10%. The results were similar for injections in

https://doi.org/10.5194/egusphere-2024-2263
Preprint. Discussion started: 9 August 2024

sensitive areas, with changes in CDNC and LWP contributing similarly and more than changes in cloud fractions to SW_CLD (Fig. S28). The changes in SW_CLD responses after aerosol injections in the sensitive areas of Equa were mainly contributed by LWP effects (~70%).

Uniform injections of sea-salt aerosols at a rate of 10^{-9} kg m^{-2} s^{-1} produced susceptibilities ($\frac{\Delta\alpha}{\Delta \ln \mathrm{AOD}}$) ranging from 0.0003 to 0.0035 in the five regions, with corresponding spatial distributions shown in Fig. 11. NP, SP, and SA regions exhibited cloud responses that were more sensitive to aerosol injections in most of the region, with susceptibilities ranging from 0.0028 to 0.0035. The Equa showed the lowest susceptibility, indicating that the system was less responsive to variations in aerosol injections. It is noteworthy that although the average susceptibility in the Asia region was 0.0013, the higher susceptibility values were concentrated in the north of 35°N, where the average susceptibility was 0.0026, similar to those of the SP region, suggesting that clouds here were more susceptible to aerosol injections. Injecting sea-salt aerosols in sensitive areas mostly resulted in cloud that were located outside the sensitive areas (Fig. S28). Injecting sea-salt aerosols in the sensitive areas of SP and SA had a greater impact on the northwest. In the sensitive areas of NP, injecting sea-salt aerosols had a larger impact on the west. In the Asia, the injection of sea-salt aerosols into the sensitive area did not fully reflect its susceptibility because we chose to calculate the sensitive areas away from the boundary, and the greatest susceptibilities in the Asia region happened to be in the northern part of the region near the boundary.

4. Discussions and conclusions

Many studies have discussed the contributions of both the direct and indirect effects of MCB. Some studies suggest that MCB primarily relies on the indirect effects, as originally conceived, i.e., injecting aerosols to brighten clouds (Jones and Haywood, 2012; Latham et al., 2012). On the other hand, other studies proposed that the direct scattering effects of aerosols may be more important (Ahlm et al., 2017; Kravitz et al., 2013; Mahfouz et al., 2023; Niemeier et al., 2013; Partanen et al., 2012). Our results indicate that the importance of both aerosol direct and indirect effects during MCB implementation depended on the injection amounts and the choice of injection regions. In cases of low sea-salt aerosol injections or the early stage of MCB implementations, changes in radiative response were mainly driven by indirect effects, causing clouds to brighten easily. As the injections of sea-salt aerosol increased, the radiative effects on clouds saturated, and the clouds were difficult to brighten. In contrast, the direct effect continued to increase linearly, leading to a subsequent decrease in the efficiencies of MCB. Partanen et al. (2012) first considered the relative importance of aerosol direct and indirect effects in MCB and preliminarily found

https://doi.org/10.5194/egusphere-2024-2263
Preprint. Discussion started: 9 August 2024

the saturated non-linear phenomenon of indirect effects at high CDNC, as well as the linear relationships between direct effects and injection amounts. Haywood et al. (2023) also found a decrease in MCB efficiency with increasing aerosol injections. Regions initially susceptible to modification gradually became less susceptible, and aerosol direct radiation effects dominated. This study emphasized and quantified these findings, showing the changing trends of direct and indirect effects with injection amounts in the different ocean regions. The best results were obtained in regions with persistent stratocumulus clouds (e.g., the oceans along the west coast of the continent), where the injected sea-salt aerosols worked together through both direct and indirect effects. However, in cloud-free or less cloudy regions, MCB implementation can achieve the goal of reflecting more sunlight through the direct scattering effect of aerosols. Considering the uncertainty in the model's resolution of clouds and the fact that, in reality, the cloud distributions were also greatly influenced by the local meteorological conditions, the direct scattering effects of sea-salt aerosols on MCB contributions were relatively certain. Therefore, in cloud-free or less cloudy regions, the direct effects of aerosols become more important.

In the early stages of Earth-System modeling studies, the MCB processes were often simulated by presetting CDNC = 375 or 1000 cm^{-3} in the lower regions of the ocean (Jones et al., 2009; Latham et al., 2008; Rasch et al., 2009). However, many follow-up studies have suggested that injections of sea-salt aerosols were difficult to produce a uniform CDNC field due to aerosol dilutions, depositions, and the dependences of the spray rate on wind speed. The CDNC was highly variable spatially, and studies have even reported reductions in CCN and CDNC caused by the injections of sea-salt aerosols (Alterskjær et al., 2012; Korhonen et al., 2010; Pringle et al., 2012). In this study, after injecting accumulation mode sea-salt aerosols at a rate of 10^{-9} kg m^{-2} s^{-1}, the average CDNC concentrations for five ocean regions ranged from 60 to 103 cm^{-3}, and the spatial distributions were uneven (Fig. 10 and Figs. S15–S18). Figure 9b indicates that the CCN in the five regions increased linearly ($R^2 = 1$) with increasing sea-salt aerosol injections, but not all of the CCN was converted to cloud droplets. After doubling the injection amounts, the regional average CDNC was 85–134 cm^{-3}, with only some grid points exceeding 200 cm^{-3} within the regions. This implies that injecting more sea-salt aerosols at this point did not result in more cloud droplets, and the conversion of CCN into cloud droplets was less efficient, which slowed the CDNC growths and tended to saturation (Fig. 9c). Alterskjær et al. (2012) similarly injected sea-salt aerosols at a rate of 10^{-9} kg m^{-2} s^{-1} and found that despite emitting sea-salt mass 70 times larger than suggested by Latham et al. (2008), the average CDNC over the ocean was below their assumed value of 375 cm^{-3}. This is mainly due to increased competitive effects, decreased maximum supersaturations, inhibitions of aerosol activations,

https://doi.org/10.5194/egusphere-2024-2263
Preprint. Discussion started: 9 August 2024

and closures of SO_4 nucleation, resulting in reduced effectiveness of sea salt injections. When Partanen et al. (2012) injected sea-salt aerosols in a Wind-adjusted way (injection amount different from this study), they found the CDNC values of 596, 650, and 784 cm^{-3} in the NP, SP, and SA regions, respectively. Injecting smaller-sized sea-salt aerosols even yielded CDNC values exceeding 1000 cm^{-3}. They concluded that such high values were mainly due to the model's overestimation of the sizes and solubilities of accumulated mode particles, with some non-activated particles forming cloud droplets. Hill and Ming (2012) increased the concentrations of sea-salt aerosols by a factor of five, resulting in an average CDNC increasing from 68 to 148 cm^{-3} between 850–925 hPa. It is noteworthy that Hill and Ming (2012) increased all modes of sea-salt aerosols, while this study only injected accumulation mode sea-salt aerosols. Many studies have reported that selecting the appropriate injection particle size was crucial for MCB (Andrejczuk et al., 2014; Hoffmann and Feingold, 2021; Partanen et al., 2012), and injecting Aitken and coarse modes may even lead to a positive forcing with CDNC decreasing (Alterskjær and Kristjánsson, 2013). However, Wood (2021) argued that particles with a geometric mean dry diameter of 30–60 nm were most effective in brightening cloud layers, and Goddard et al. (2022) similarly found that injecting Aitken mode sea-salt aerosols generated larger radiative flux changes compared to accumulation mode (8.4 W m^{-2} versus 3.1 W m^{-2}). There were still considerable discussions about choosing the appropriate aerosol particle sizes during the implementation of MCB, with different models and parameterization schemes providing different recommendations. The sensitivity of MCB to particle size was not considered in this paper and was left for future research.

In this study the injection of 10^{-9} kg m^{-2} s^{-1} accumulation mode sea-salt aerosols increased cloud albedo in the five ocean regions by 0.13–0.20, with a maximum of more than 0.3. After doubling the injection amounts, the regional average cloud albedo could reach 0.45–0.55, representing a cloud albedo change of 0.15–0.24 (Fig. 9d). These values achieved the targeted cloud albedo change as envisioned in previous studies. Bower et al. (2006) suggested that to compensate for the warming associated with doubling atmospheric CO_2 concentrations, a cloud albedo change of 0.16 was needed in three stratocumulus cloud regions (off the west coast of Africa and North and South America, representing 3% of global cloud cover). Wood (2021) proposed seeding Aitken mode particles in approximately 9% of the ocean to achieve a corresponding cloud albedo increase of 0.16. It was also suggested that injecting sea-salt aerosols in a clean, undisturbed state would produce more brightening. Fig. 9d confirms this finding, indicating that clouds are more likely to brighten in the early stages of sea-salt aerosol injection, and the efficiency of cloud brightening decreases with increasing injection amounts. Kravitz et al. (2014)

https://doi.org/10.5194/egusphere-2024-2263
Preprint. Discussion started: 9 August 2024

achieved a maximum cloud albedo change of 0.23 by injecting CCN in the Arctic region. For the global implementation of MCB, global cloud albedo increases of 0.02 (Bower et al., 2006), 0.062 (Latham et al., 2008), or 0.074 (Lenton and Vaughan, 2009) were estimated. The change in cloud albedo is influenced by the properties of injected particles and the injection strategies. Jenkins et al. (2013) proposed that the optimal injection time should be in the early morning over weakly precipitating cloud regions, achieving a cloud albedo increase of 0.28. Goddard et al. (2022), simulating injecting accumulation mode sea-salt aerosols in the central Gulf of Mexico, and achieved a simulated cloud albedo change of approximately 0.1 in the main impact region, while switching to Aitken mode injection resulted in a cloud albedo change of up to 0.35.

The contributions of the change in cloud fractions to the SW_CLD responses in this study were small, which was consistent with the results of Goddard et al. (2022). However, many observational studies indicate that the contribution of cloud fraction to the shortwave radiative forcing should be similar to those of the CDNC and LWP (Chen et al., 2014; Rosenfeld et al., 2019). Goddard et al. (2022) believe that this was due to the fact that the regional atmosphere was wetter during the simulation periods and that the relative contributions of changes in cloud fraction to the SW_CLD response would be expected to increase in drier months (Fig. S29). Three of the five ocean regions in this study (SA, SP, and NP) were much drier and more stable than the Gulf of Mexico simulated by Goddard et al. (2022). Furthermore, when we switched to conducting the experiments again in the dry months of the same year, the contribution of cloud fraction to SW_CLD did not change much, remaining at ~10%. We believe that this might be a difference due to the parameterization scheme or resolution of the model. Liu et al. (2020) simulated with WRF–Chem model and found that the cloud fraction susceptibilities to aerosols in Morrison scheme and the Lin scheme were only about half of those observed by Moderate Resolution Imaging Spectroradiometer (MODIS). The neglected sub-gridded clouds in the 12-km resolution simulations might lead to an underestimation of the radiative effects of clouds (Yu et al., 2014). In addition, cloud fractions were more commonly underestimated in the model (Glotfelty et al., 2019), and using an updated parameterization scheme that accounts for sub-grid condensation might improve the model's ability to resolve clouds (Zhao et al., 2023). The effects of finer resolution and more parameterization schemes on aerosol-cloud interactions still need to be verified. Considering the difficulties of modeling to accurately capture the effects of cloud fractions on radiation, the actual effects of MCB may be underestimated. The radiative results obtained in this study may represent a lower limit to cooling.

This study provided quantifiable data on cloud and radiation changes for the implementation of MCB

https://doi.org/10.5194/egusphere-2024-2263
Preprint. Discussion started: 9 August 2024

over the regional oceans, and an optimization scheme on the injection strategy by adjusting the injection amounts and selecting sensitive areas. It is noteworthy that different parameterization schemes, models, and resolutions can influence results, especially the cloud feedback on the injected sea-salt aerosols, which is a major reason for discrepancies between models (Stjern et al., 2018). In Earth-system model studies, there has been a rich discussion of the climate and ecological impacts of the MCB with the Geoengineering Model Intercomparison Project (GeoMIP) under the same framework. However, there is still a lack of a unified framework for mid-scale MCB research.

Data and code availability

The computational code for cloud and radiation can be found in the code publicly available from Goddard et al. (2022). The model results are available upon request.

Supplemental information.

The supplementary information related to this article is available online.

Competing interests. The authors declare that they have no conflict of interest.

Acknowledgements. The study was motivated by the need to assess the susceptibility of clouds over locations such as the Great Barrier Reef, where a marine cloud brightening experiment is being performed by the Reef Restoration and Adaptation Program of the Southern Cross University. The authors would like to thank P. B. Goddard for his open-source computing methods and codes.

Financial supports. This work was supported by National Natural Science Foundation of China (No. 72361137007, 42175084, 21577126, 41561144004), Ministry of Science and Technology of China (No. 2016YFC0202702, 2018YFC0213506, 2018YFC0213503) and National Air Pollution Control Key Issues Research Program (No. DQGG0107).

References

Ahlm, L., Jones, A., Stjern, C. W., Muri, H., Kravitz, B., and Kristjánsson, J. E.: Marine cloud brightening – as effective without clouds, Atmospheric Chemistry and Physics, 17, 13071–13087, https://doi.org/10.5194/acp-17-13071-2017, 2017.

Albrecht, B. A.: Aerosols, Cloud Microphysics, and Fractional Cloudiness, Science, 245, 1227–1230, https://doi.org/10.1126/science.245.4923.1227, 1989.

Alterskjær, K. and Kristjánsson, J. E.: The sign of the radiative forcing from marine cloud brightening depends on both particle size and injection amount, Geophysical Research Letters, 40, 210–215, https://doi.org/10.1029/2012GL054286, 2013.

Alterskjær, K., Kristjánsson, J. E., and Seland, Ø.: Sensitivity to deliberate sea salt seeding of marine clouds – observations and model simulations, Atmospheric Chemistry and Physics, 12, 2795–2807, https://doi.org/10.5194/acp-12-2795-2012, 2012.

Andrejczuk, M., Gadian, A., and Blyth, A.: Numerical simulations of stratocumulus cloud response to aerosol perturbation, Atmospheric Research, 140–141, 76–84, https://doi.org/10.1016/j.atmosres.2014.01.006, 2014.

Binkowski, F. S. and Roselle, S. J.: Models-3 Community Multiscale Air Quality (CMAQ) model aerosol component 1. Model description, Journal of Geophysical Research: Atmospheres, 108, https://doi.org/10.1029/2001JD001409, 2003.

Bower, K., Choularton, T., Latham, J., Sahraei, J., and Salter, S.: Computational assessment of a proposed technique for global warming mitigation via albedo-enhancement of marine stratocumulus clouds, Atmospheric Research, 82, 328–

https://doi.org/10.5194/egusphere-2024-2263
Preprint. Discussion started: 9 August 2024

336, https://doi.org/10.1016/j.atmosres.2005.11.013, 2006.

Carlton, A. G. and Baker, K. R.: Photochemical Modeling of the Ozark Isoprene Volcano: MEGAN, BEIS, and Their Impacts on Air Quality Predictions, Environ. Sci. Technol., 45, 4438–4445, https://doi.org/10.1021/es200050x, 2011.

Chen, Y.-C., Christensen, M. W., Xue, L., Sorooshian, A., Stephens, G. L., Rasmussen, R. M., and Seinfeld, J. H.: Occurrence of lower cloud albedo in ship tracks, Atmospheric Chemistry and Physics, 12, 8223–8235, https://doi.org/10.5194/acp-12-8223-2012, 2012.

Chen, Y.-C., Christensen, M. W., Stephens, G. L., and Seinfeld, J. H.: Satellite-based estimate of global aerosol–cloud radiative forcing by marine warm clouds, Nature Geosci, 7, 643–646, https://doi.org/10.1038/ngeo2214, 2014.

Christensen, M. W., Jones, W. K., and Stier, P.: Aerosols enhance cloud lifetime and brightness along the stratus-to-cumulus transition, Proceedings of the National Academy of Sciences, 117, 17591–17598, https://doi.org/10.1073/pnas.1921231117, 2020.

Forster, P., Ramaswamy, V., Artaxo, P., Berntsen, T., Betts, R., Fahey, D. W., Haywood, J., Lean, J., Lowe, D. C., Raga, G., Schulz, M., Dorland, R. V., Bodeker, G., Etheridge, D., Foukal, P., Fraser, P., Geller, M., Joos, F., Keeling, C. D., Keeling, R., Kinne, S., Lassey, K., Oram, D., O'Shaughnessy, K., Ramankutty, N., Reid, G., Rind, D., Rosenlof, K., Sausen, R., Schwarzkopf, D., Solanki, S. K., Stenchikov, G., Stuber, N., Takemura, T., Textor, C., Wang, R., Weiss, R., Whorf, T., Nakajima, T., Ramanathan, V., Ramaswamy, V., Artaxo, P., Berntsen, T., Betts, R., Fahey, D. W., Haywood, J., Lean, J., Lowe, D. C., Myhre, G., Nganga, J., Prinn, R., Raga, G., Schulz, M., and Dorland, R. V.: Changes in Atmospheric Constituents and in Radiative Forcing, 2007.

Ghan, S. J., Liu, X., Easter, R. C., Zaveri, R., Rasch, P. J., Yoon, J.-H., and Eaton, B.: Toward a Minimal Representation of Aerosols in Climate Models: Comparative Decomposition of Aerosol Direct, Semidirect, and Indirect Radiative Forcing, Journal of Climate, 25, 6461–6476, https://doi.org/10.1175/JCLI-D-11-00650.1, 2012.

Glotfelty, T., Alapaty, K., He, J., Hawbecker, P., Song, X., and Zhang, G.: The Weather Research and Forecasting Model with Aerosol–Cloud Interactions (WRF-ACI): Development, Evaluation, and Initial Application, Mon Weather Rev, 147, 1491–1511, https://doi.org/10.1175/MWR-D-18-0267.1, 2019.

Goddard, P. B., Kravitz, B., MacMartin, D. G., and Wang, H.: The Shortwave Radiative Flux Response to an Injection of Sea Salt Aerosols in the Gulf of Mexico, Journal of Geophysical Research: Atmospheres, 127, e2022JD037067, https://doi.org/10.1029/2022JD037067, 2022.

Gong, S. L.: A parameterization of sea-salt aerosol source function for sub- and super-micron particles, Global Biogeochemical Cycles, 17, https://doi.org/10.1029/2003GB002079, 2003.

Grythe, H., Ström, J., Krejci, R., Quinn, P., and Stohl, A.: A review of sea-spray aerosol source functions using a large global set of sea salt aerosol concentration measurements, Atmospheric Chemistry and Physics, 14, 1277–1297, https://doi.org/10.5194/acp-14-1277-2014, 2014.

Haywood, J. M., Jones, A., Jones, A. C., and Rasch, P. J.: Climate Intervention using marine cloud brightening (MCB) compared with stratospheric aerosol injection (SAI) in the UKESM1 climate model, EGUsphere, 1–38, https://doi.org/10.5194/egusphere-2023-1611, 2023.

Hill, S. and Ming, Y.: Nonlinear climate response to regional brightening of tropical marine stratocumulus, Geophysical Research Letters, 39, https://doi.org/10.1029/2012GL052064, 2012.

https://doi.org/10.5194/egusphere-2024-2263
Preprint. Discussion started: 9 August 2024

Hoffmann, F. and Feingold, G.: Cloud Microphysical Implications for Marine Cloud Brightening: The Importance of the Seeded Particle Size Distribution, Journal of the Atmospheric Sciences, 78, 3247–3262, https://doi.org/10.1175/JAS-D-21-0077.1, 2021.

Horowitz, H. M., Holmes, C., Wright, A., Sherwen, T., Wang, X., Evans, M., Huang, J., Jaeglé, L., Chen, Q., Zhai, S., and Alexander, B.: Effects of Sea Salt Aerosol Emissions for Marine Cloud Brightening on Atmospheric Chemistry: Implications for Radiative Forcing, Geophysical Research Letters, 47, e2019GL085838, https://doi.org/10.1029/2019GL085838, 2020.

Janssens-Maenhout, G., Crippa, M., Guizzardi, D., Dentener, F., Muntean, M., Pouliot, G., Keating, T., Zhang, Q., Kurokawa, J., Wankmüller, R., Denier van der Gon, H., Kuenen, J. J. P., Klimont, Z., Frost, G., Darras, S., Koffi, B., and Li, M.: HTAP_v2.2: a mosaic of regional and global emission grid maps for 2008 and 2010 to study hemispheric transport of air pollution, Atmospheric Chemistry and Physics, 15, 11411–11432, https://doi.org/10.5194/acp-15-11411-2015, 2015.

Jenkins, A. K. L., Forster, P. M., and Jackson, L. S.: The effects of timing and rate of marine cloud brightening aerosol injection on albedo changes during the diurnal cycle of marine stratocumulus clouds, Atmospheric Chemistry and Physics, 13, 1659–1673, https://doi.org/10.5194/acp-13-1659-2013, 2013.

Jones, A. and Haywood, J. M.: Sea-spray geoengineering in the HadGEM2-ES earth-system model: radiative impact and climate response, Atmospheric Chemistry and Physics, 12, 10887–10898, https://doi.org/10.5194/acp-12-10887-2012, 2012.

Jones, A., Haywood, J., and Boucher, O.: Climate impacts of geoengineering marine stratocumulus clouds, Journal of Geophysical Research: Atmospheres, 114, https://doi.org/10.1029/2008JD011450, 2009.

Kelly, J. T., Bhave, P. V., Nolte, C. G., Shankar, U., and Foley, K. M.: Simulating emission and chemical evolution of coarse sea-salt particles in the Community Multiscale Air Quality (CMAQ) model, Geoscientific Model Development, 3, 257–273, https://doi.org/10.5194/gmd-3-257-2010, 2010.

Korhonen, H., Carslaw, K. S., and Romakkaniemi, S.: Enhancement of marine cloud albedo via controlled sea spray injections: a global model study of the influence of emission rates, microphysics and transport, Atmospheric Chemistry and Physics, 10, 4133–4143, https://doi.org/10.5194/acp-10-4133-2010, 2010.

Kravitz, B., Forster, P. M., Jones, A., Robock, A., Alterskjær, K., Boucher, O., Jenkins, A. K. L., Korhonen, H., Kristjánsson, J. E., Muri, H., Niemeier, U., Partanen, A.-I., Rasch, P. J., Wang, H., and Watanabe, S.: Sea spray geoengineering experiments in the geoengineering model intercomparison project (GeoMIP): Experimental design and preliminary results, Journal of Geophysical Research: Atmospheres, 118, 11,175-11,186, https://doi.org/10.1002/jgrd.50856, 2013.

Kravitz, B., Wang, H., Rasch, P. J., Morrison, H., and Solomon, A. B.: Process-model simulations of cloud albedo enhancement by aerosols in the Arctic, Phil. Trans. R. Soc. A., 372, 20140052, https://doi.org/10.1098/rsta.2014.0052, 2014.

Latham, J., Rasch, P., Chen, C.-C., Kettles, L., Gadian, A., Gettelman, A., Morrison, H., Bower, K., and Choularton, T.: Global temperature stabilization via controlled albedo enhancement of low-level maritime clouds, Philosophical Transactions of the Royal Society A: Mathematical, Physical and Engineering Sciences, 366, 3969–3987, https://doi.org/10.1098/rsta.2008.0137, 2008.

https://doi.org/10.5194/egusphere-2024-2263
Preprint. Discussion started: 9 August 2024

Latham, J., Bower, K., Choularton, T., Coe, H., Connolly, P., Cooper, G., Craft, T., Foster, J., Gadian, A., Galbraith, L., Iacovides, H., Johnston, D., Launder, B., Leslie, B., Meyer, J., Neukermans, A., Ormond, B., Parkes, B., Rasch, P., Rush, J., Salter, S., Stevenson, T., Wang, H., Wang, Q., and Wood, R.: Marine cloud brightening, Philosophical Transactions of the Royal Society A: Mathematical, Physical and Engineering Sciences, 370, 4217–4262, https://doi.org/10.1098/rsta.2012.0086, 2012.

Latham, J., Gadian, A., Fournier, J., Parkes, B., Wadhams, P., and Chen, J.: Marine cloud brightening: regional applications, Philosophical Transactions of the Royal Society A: Mathematical, Physical and Engineering Sciences, 372, 20140053, https://doi.org/10.1098/rsta.2014.0053, 2014.

Lenton, T. M. and Vaughan, N. E.: The radiative forcing potential of different climate geoengineering options, Atmospheric Chemistry and Physics, 9, 5539–5561, https://doi.org/10.5194/acp-9-5539-2009, 2009.

Liu, F., Mao, F., Rosenfeld, D., Pan, Z., Zang, L., Zhu, Y., Yin, J., and Gong, W.: Opposing comparable large effects of fine aerosols and coarse sea spray on marine warm clouds, Commun Earth Environ, 3, 1–9, https://doi.org/10.1038/s43247-022-00562-y, 2022.

Liu, Z., Wang, M., Rosenfeld, D., Zhu, Y., Bai, H., Cao, Y., and Liang, Y.: Evaluation of Cloud and Precipitation Response to Aerosols in WRF-Chem With Satellite Observations, Journal of Geophysical Research: Atmospheres, 125, e2020JD033108, https://doi.org/10.1029/2020JD033108, 2020.

Mahfouz, N. G. A., Hill, S. A., Guo, H., and Ming, Y.: The Radiative and Cloud Responses to Sea Salt Aerosol Engineering in GFDL Models, Geophysical Research Letters, 50, e2022GL102340, https://doi.org/10.1029/2022GL102340, 2023.

Mengel, M., Nauels, A., Rogelj, J., and Schleussner, C.-F.: Committed sea-level rise under the Paris Agreement and the legacy of delayed mitigation action, Nat Commun, 9, 601, https://doi.org/10.1038/s41467-018-02985-8, 2018.

Monahan, E. C., Spiel, D. E., and Davidson, K. L.: A Model of Marine Aerosol Generation Via Whitecaps and Wave Disruption, in: Oceanic Whitecaps: And Their Role in Air-Sea Exchange Processes, edited by: Monahan, E. C. and Niocaill, G. M., Springer Netherlands, Dordrecht, 167–174, https://doi.org/10.1007/978-94-009-4668-2_16, 1986.

Morrison, H., Thompson, G., and Tatarskii, V.: Impact of Cloud Microphysics on the Development of Trailing Stratiform Precipitation in a Simulated Squall Line: Comparison of One- and Two-Moment Schemes, Monthly Weather Review, 137, 991–1007, https://doi.org/10.1175/2008mwr2556.1, 2009.

Niemeier, U., Schmidt, H., Alterskjær, K., and Kristjánsson, J. E.: Solar irradiance reduction via climate engineering: Impact of different techniques on the energy balance and the hydrological cycle, Journal of Geophysical Research: Atmospheres, 118, 11,905-11,917, https://doi.org/10.1002/2013JD020445, 2013.

Partanen, A.-I., Kokkola, H., Romakkaniemi, S., Kerminen, V.-M., Lehtinen, K. E. J., Bergman, T., Arola, A., and Korhonen, H.: Direct and indirect effects of sea spray geoengineering and the role of injected particle size, Journal of Geophysical Research: Atmospheres, 117, https://doi.org/10.1029/2011JD016428, 2012.

Paulot, F., Paynter, D., Winton, M., Ginoux, P., Zhao, M., and Horowitz, L. W.: Revisiting the Impact of Sea Salt on Climate Sensitivity, Geophysical Research Letters, 47, e2019GL085601, https://doi.org/10.1029/2019GL085601, 2020.

Pleim, J. E.: A Combined Local and Nonlocal Closure Model for the Atmospheric Boundary Layer. Part I: Model Description and Testing, Journal of Applied Meteorology and Climatology, 46, 1383–1395,

https://doi.org/10.5194/egusphere-2024-2263
Preprint. Discussion started: 9 August 2024

https://doi.org/10.1175/jam2539.1, 2007.

Pringle, K. J., Carslaw, K. S., Fan, T., Mann, G. W., Hill, A., Stier, P., Zhang, K., and Tost, H.: A multi-model assessment of the impact of sea spray geoengineering on cloud droplet number, Atmospheric Chemistry and Physics, 12, 11647–11663, https://doi.org/10.5194/acp-12-11647-2012, 2012.

Quaas, J., Boucher, O., Bellouin, N., and Kinne, S.: Satellite-based estimate of the direct and indirect aerosol climate forcing, Journal of Geophysical Research: Atmospheres, 113, https://doi.org/10.1029/2007JD008962, 2008.

Ramaswamy, V., Boucher, O., Haigh, J., Hauglustaine, D., Haywood, J., Myhre, G., Nakajima, T., Shi, G. Y., Solomon, S., Betts, R., Charlson, R., Chuang, C., Daniel, J. S., Joos, F., and Srinivasan, J.: Radiative Forcing of Climate Change, 2001.

Rasch, P. J., Latham, J., and Chen, C.-C. (Jack): Geoengineering by cloud seeding: influence on sea ice and climate system, Environ. Res. Lett., 4, 045112, https://doi.org/10.1088/1748-9326/4/4/045112, 2009.

Rosenfeld, Daniel, Sherwood, Steven, Wood, Robert, Donner, and Leo: Climate Effects of Aerosol-Cloud Interactions., Science, https://doi.org/10.1126/science.1247490, 2014.

Rosenfeld, D., Zhu, Y., Wang, M., Zheng, Y., Goren, T., and Yu, S.: Aerosol-driven droplet concentrations dominate coverage and water of oceanic low-level clouds, Science, 363, eaav0566, https://doi.org/10.1126/science.aav0566, 2019.

Salter, S., Sortino, G., and Latham, J.: Sea-going hardware for the cloud albedo method of reversing global warming, Philosophical Transactions of the Royal Society A: Mathematical, Physical and Engineering Sciences, 366, 3989–4006, https://doi.org/10.1098/rsta.2008.0136, 2008.

Stjern, C. W., Muri, H., Ahlm, L., Boucher, O., Cole, J. N. S., Ji, D., Jones, A., Haywood, J., Kravitz, B., Lenton, A., Moore, J. C., Niemeier, U., Phipps, S. J., Schmidt, H., Watanabe, S., and Kristjánsson, J. E.: Response to marine cloud brightening in a multi-model ensemble, Atmospheric Chemistry and Physics, 18, 621–634, https://doi.org/10.5194/acp-18-621-2018, 2018.

Stuart, G. S., Stevens, R. G., Partanen, A.-I., Jenkins, A. K. L., Korhonen, H., Forster, P. M., Spracklen, D. V., and Pierce, J. R.: Reduced efficacy of marine cloud brightening geoengineering due to in-plume aerosol coagulation: parameterization and global implications, Atmospheric Chemistry and Physics, 13, 10385–10396, https://doi.org/10.5194/acp-13-10385-2013, 2013.

Twomey, S.: Pollution and the planetary albedo, Atmospheric Environment (1967), 8, 1251–1256, https://doi.org/10.1016/0004-6981(74)90004-3, 1974.

Visioni, D., Kravitz, B., Robock, A., Tilmes, S., Haywood, J., Boucher, O., Lawrence, M., Irvine, P., Niemeier, U., Xia, L., Chiodo, G., Lennard, C., Watanabe, S., Moore, J. C., and Muri, H.: Opinion: The scientific and community-building roles of the Geoengineering Model Intercomparison Project (GeoMIP) – past, present, and future, Atmospheric Chemistry and Physics, 23, 5149–5176, https://doi.org/10.5194/acp-23-5149-2023, 2023.

Wang, K., Zhang, Y., Yu, S., Wong, D. C., Pleim, J., Mathur, R., Kelly, J. T., and Bell, M.: A comparative study of two-way and offline coupled WRF v3.4 and CMAQ v5.0.2 over the contiguous US: performance evaluation and impacts of chemistry–meteorology feedbacks on air quality, Geoscientific Model Development, 14, 7189–7221, https://doi.org/10.5194/gmd-14-7189-2021, 2021.

Wong, D. C., Pleim, J., Mathur, R., Binkowski, F., Otte, T., Gilliam, R., Pouliot, G., Xiu, A., Young, J. O., and Kang, D.:

https://doi.org/10.5194/egusphere-2024-2263
Preprint. Discussion started: 9 August 2024

WRF-CMAQ two-way coupled system with aerosol feedback: software development and preliminary results, Geoscientific Model Development, 5, 299–312, https://doi.org/10.5194/gmd-5-299-2012, 2012.

Wood, R.: Assessing the potential efficacy of marine cloud brightening for cooling Earth using a simple heuristic model, Atmospheric Chemistry and Physics, 21, 14507–14533, https://doi.org/10.5194/acp-21-14507-2021, 2021.

Yu, S., Mathur, R., Pleim, J., Wong, D., Gilliam, R., Alapaty, K., Zhao, C., and Liu, X.: Aerosol indirect effect on the grid-scale clouds in the two-way coupled WRF–CMAQ: model description, development, evaluation and regional analysis, Atmospheric Chemistry and Physics, 14, 11247–11285, https://doi.org/10.5194/acp-14-11247-2014, 2014.

Zhang, K. M., Knipping, E. M., Wexler, A. S., Bhave, P. V., and Tonnesen, G. S.: Size distribution of sea-salt emissions as a function of relative humidity, Atmospheric Environment, 39, 3373–3379, https://doi.org/10.1016/j.atmosenv.2005.02.032, 2005.

Zhao, D., Lin, Y., Dong, W., Qin, Y., Chu, W., Yang, K., Letu, H., and Huang, L.: Alleviated WRF Summer Wet Bias Over the Tibetan Plateau Using a New Cloud Macrophysics Scheme, Journal of Advances in Modeling Earth Systems, 15, e2023MS003616, https://doi.org/10.1029/2023MS003616, 2023.

Zhao, G., Zhao, C., Kuang, Y., Bian, Y., Tao, J., Shen, C., and Yu, Y.: Calculating the aerosol asymmetry factor based on measurements from the humidified nephelometer system, Atmospheric Chemistry and Physics, 18, 9049–9060, https://doi.org/10.5194/acp-18-9049-2018, 2018.

Zhao, M., Cao, L., Duan, L., Bala, G., and Caldeira, K.: Climate More Responsive to Marine Cloud Brightening Than Ocean Albedo Modification: A Model Study, Journal of Geophysical Research: Atmospheres, 126, e2020JD033256, https://doi.org/10.1029/2020JD033256, 2021.

https://doi.org/10.5194/egusphere-2024-2263
Preprint. Discussion started: 9 August 2024

Table 1. Differences (Exp - Base) in SW_TOT, SW_CLD, SW_AER and SW_AER_CLR at the TOA due to the injection of sea-salt aerosols in different strategies in five ocean regions.

Strategies	Areas	SW_TOT ($W m^{-2}$)	SW_CLD ($W m^{-2}$)	SW_AER ($W m^{-2}$)	SW_AER_CLR ($W m^{-2}$)
Natural×5	Asia	0.60	0.49	0.11	0.16
	NP	2.08	1.96	0.11	0.19
	Equa	0.06	-0.01	0.07	0.07
	SP	1.55	1.46	0.08	0.14
	SA	1.43	1.32	0.11	0.16
Wind-adjusted	Asia	4.02	2.09	1.93	2.30
	NP	8.47	6.89	1.59	2.35
	Equa	1.35	0.17	1.18	1.21
	SP	7.75	5.94	1.81	2.57
	SA	7.91	5.86	2.05	2.83
10^{-9} kg m^{-2} s^{-1}	Asia	17.34	4.40	12.94	15.35
	NP	23.11	13.41	9.70	14.51
	Equa	10.96	0.54	10.42	10.68
	SP	24.50	10.73	13.77	18.67
	SA	22.36	11.27	11.08	15.33
10^{-9} kg m^{-2} s^{-1} in the sensitive area	Asia	0.65	0.16	0.49	0.60
	NP	2.69	2.01	0.68	0.97
	Equa	0.74	0.10	0.64	0.65
	SP	3.27	2.24	1.04	1.35
	SA	1.81	1.20	0.61	0.79
Fixed-wind-adjusted	Asia	7.21	3.21	3.99	5.14
	NP	16.07	11.07	5.00	7.73
	Equa	5.00	0.48	4.53	4.72
	SP	16.40	9.81	6.59	9.76
	SA	19.78	10.79	8.98	12.54

Note: SW_TOT is upward shortwave radiative flux at the TOA for all-sky conditions. The response of SW_TOT to the sea-salt aerosols injection can be separated into the influence of the cloud radiative effect (SW_CLD, where the influence of the aerosol is excluded) and the influence of the aerosol direct scattering effect (SW_AER) in the presence of clouds. That is, $SW\_TOT = SW\_CLD + SW\_AER$. The SW_AER_CLR is the response of aerosol direct scattering to the upward shortwave radiative flux at the TOA under clear skies.

https://doi.org/10.5194/egusphere-2024-2263
Preprint. Discussion started: 9 August 2024

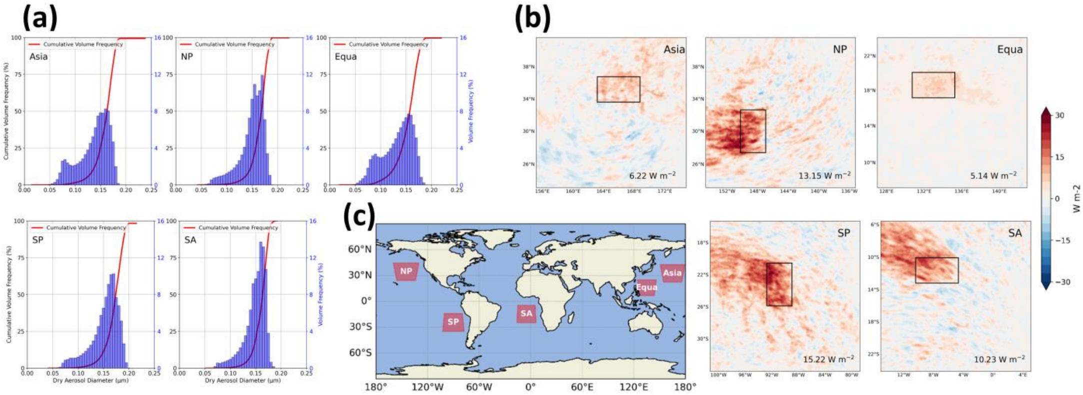

Figure 1. Injecting sea-salt aerosols into five open sea regions to simulate the implementation of MCB geoengineering. (**a**) The cumulative volume frequency of increased aerosol dry particle size. (**b**) Differences (Exp - Base) in the spatial distribution of the TOA upward shortwave radiative flux response (SW_TOT) resulting from uniform injection of 10^{-9} kg m^{-2} s^{-1} sea-salt aerosol in sensitive areas in five ocean regions, with SW_TOT response values resulting only in sensitive areas labeled in the lower right corner. Black rectangles are sensitive areas. (**c**) Location of the five ocean modeling domains.

https://doi.org/10.5194/egusphere-2024-2263
Preprint. Discussion started: 9 August 2024

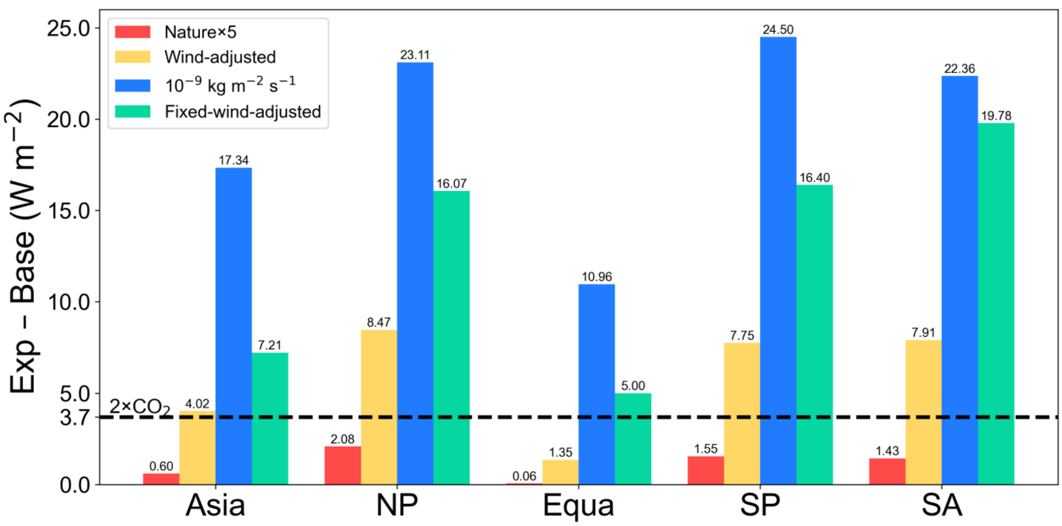

Figure 2. Differences in SW_TOT due to the injection of sea-salt aerosols in different ways in five ocean regions. The black dashed line is the radiative flux response required to offset the 3.7 W m^{-2} radiative forcing caused by the doubling of atmospheric CO_2 concentrations since industrialization.

https://doi.org/10.5194/egusphere-2024-2263
Preprint. Discussion started: 9 August 2024

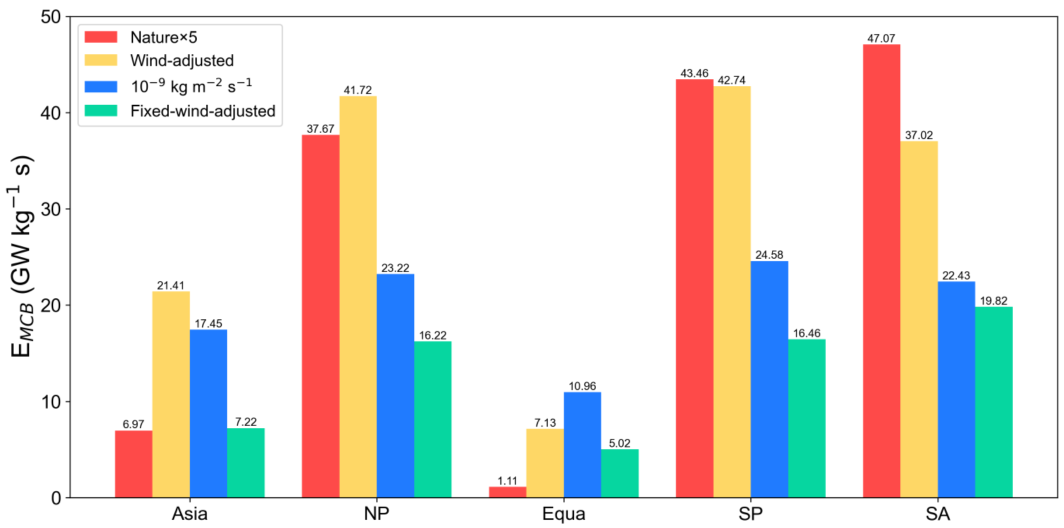

Figure 3. The MCB efficiency (E_{MCB}) after injection of sea-salt aerosols in different strategies in five sea areas.

https://doi.org/10.5194/egusphere-2024-2263
Preprint. Discussion started: 9 August 2024

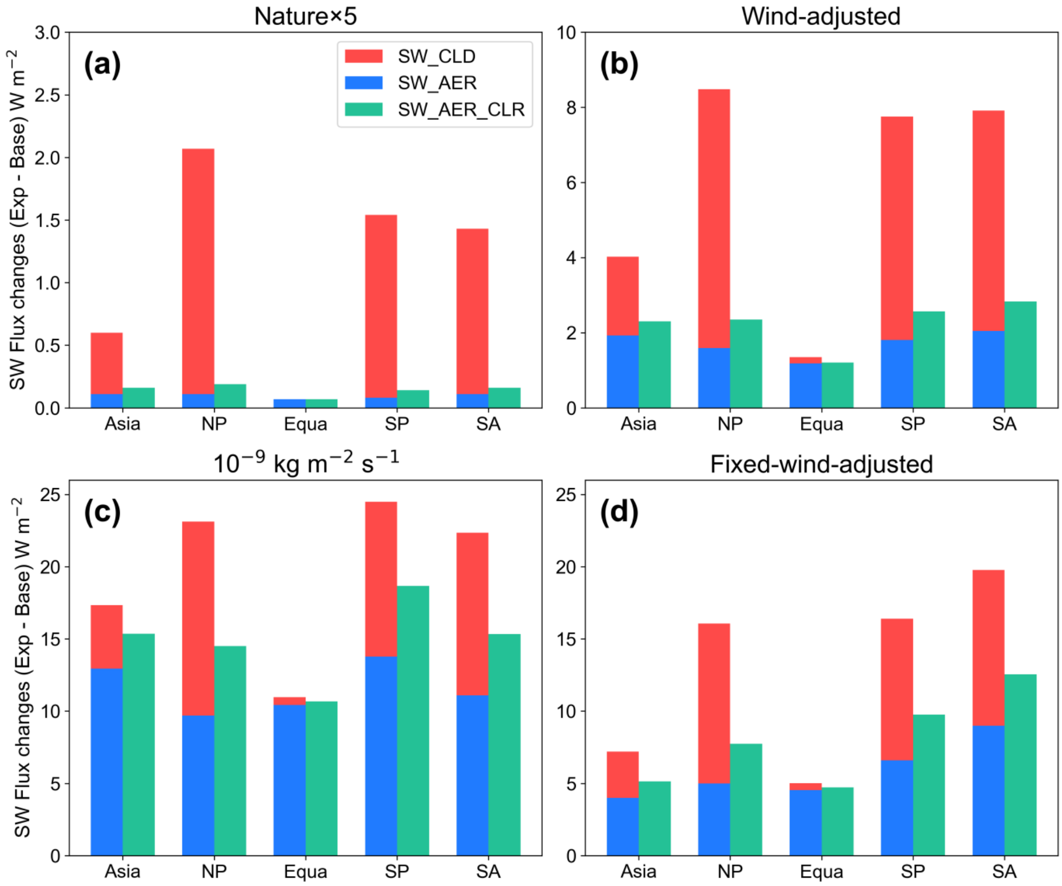

Figure 4. Decomposition of the upward shortwave radiative fluxes at the TOA due to the different ways of injecting sea-salt aerosols in the five regions. Note that the vertical coordinate ranges are not consistent.

https://doi.org/10.5194/egusphere-2024-2263
Preprint. Discussion started: 9 August 2024

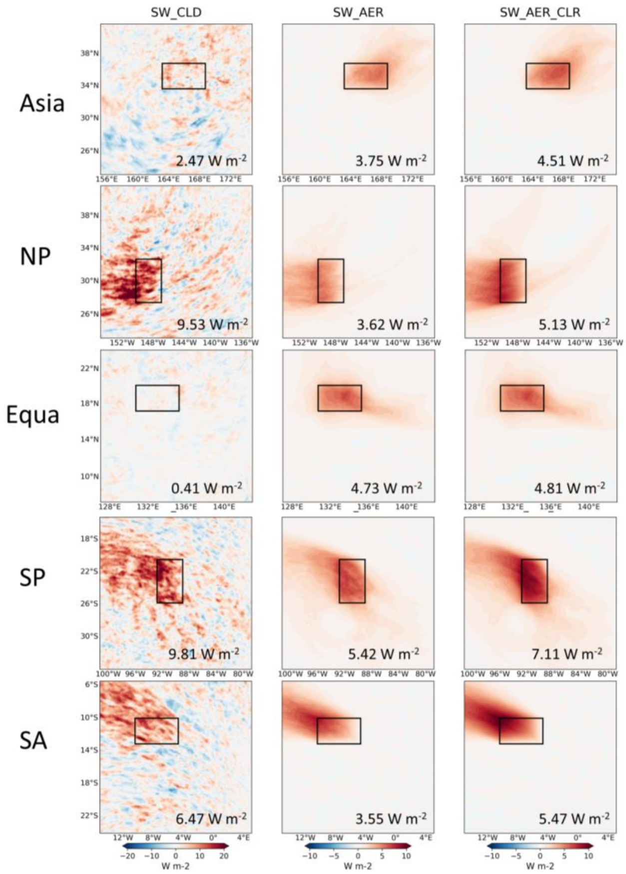

Figure 5. Spatial distribution of SW_CLD (first column), SW_AER (second column), and SW_AER_CLR (third column) responses resulting from the injection of 10^{-9} kg m^{-2} s^{-1} sea-salt aerosols in the sensitive areas over five ocean regions. The values of the radiative flux responses generated only in the sensitive area are labeled in the lower right corner. The black rectangles are sensitive areas.

https://doi.org/10.5194/egusphere-2024-2263
Preprint. Discussion started: 9 August 2024

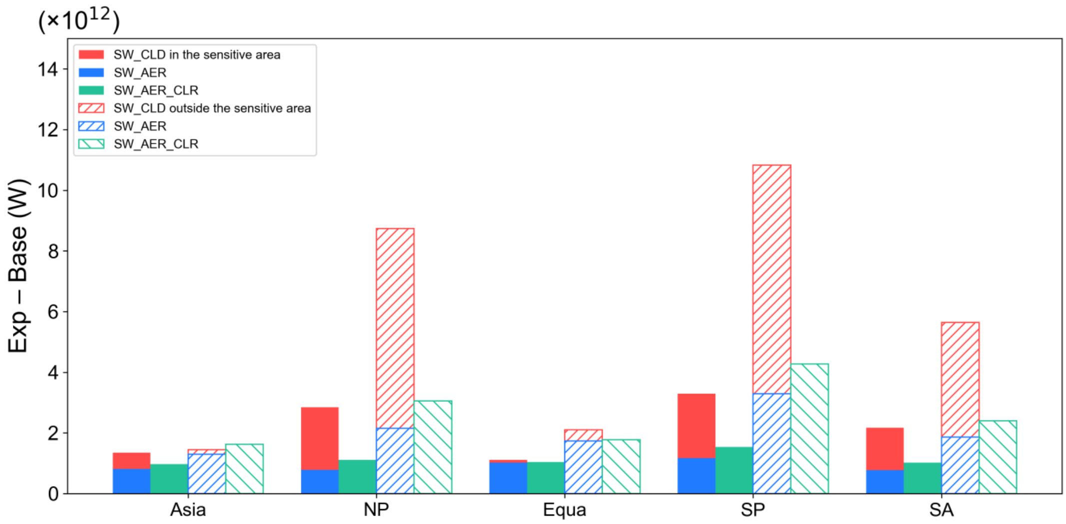

Figure 6. Total SW_CLD, SW_AER, and SW_AER_CLR responses resulting from the injection of 10^{-9} kg m^{-2} s^{-1} sea-salt aerosols within the sensitive areas of the five regions. The solid columns indicate the total radiative response calculated for aerosol injection within the sensitive areas. Columns filled with a slash style indicate the total radiative response outside the sensitive areas.

https://doi.org/10.5194/egusphere-2024-2263
Preprint. Discussion started: 9 August 2024

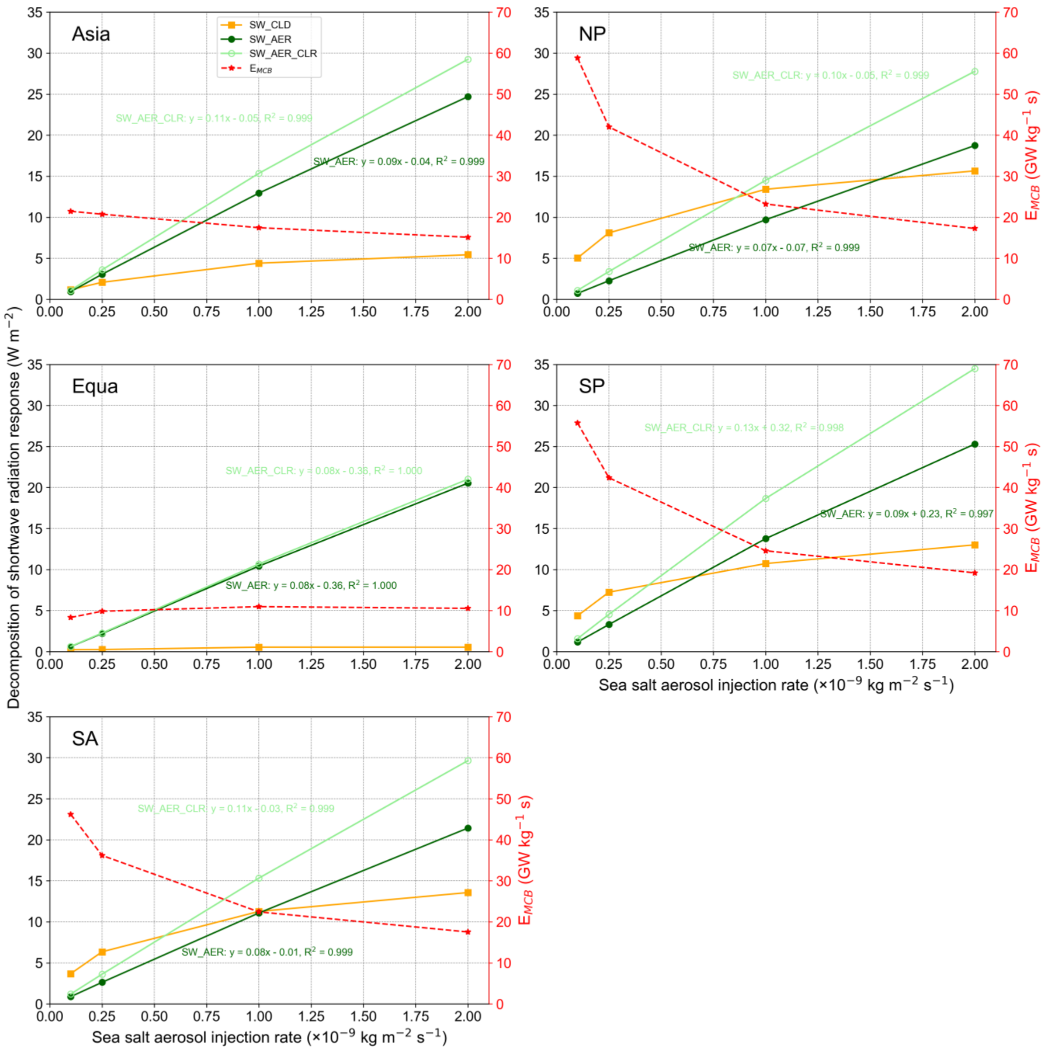

Figure 7. Changes in SW_CLD, SW_AER, and SW_AER_CLR radiative responses due to sea-salt aerosols uniformly injected in varying amounts in five ocean regions, and corresponding changes in E_{MCB}. SW_AER and SW_AER_CLR are labeled with the results of the corresponding linear regression analysis.

https://doi.org/10.5194/egusphere-2024-2263
Preprint. Discussion started: 9 August 2024

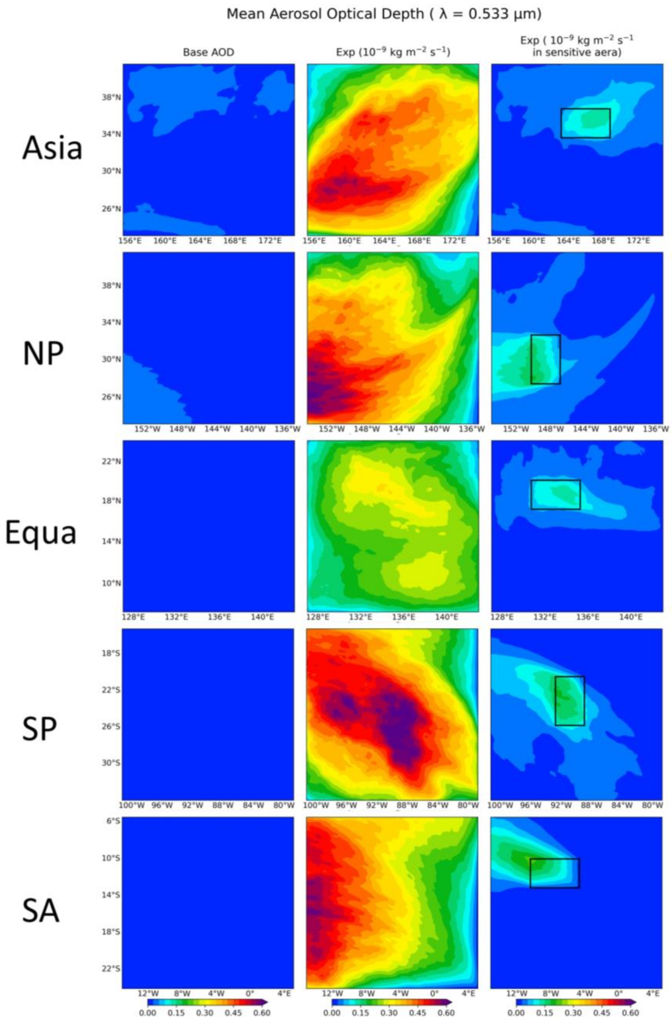

Figure 8. Spatial distribution of mean AOD (λ = 0.533 μm) for five ocean regions. The first column is the AOD for Base, the second column is the AOD after uniform injection at 10^{-9} kg m^{-2} s^{-1}, and the third column is the AOD after uniform injection in sensitive areas. The black rectangles are sensitive areas.

https://doi.org/10.5194/egusphere-2024-2263
Preprint. Discussion started: 9 August 2024

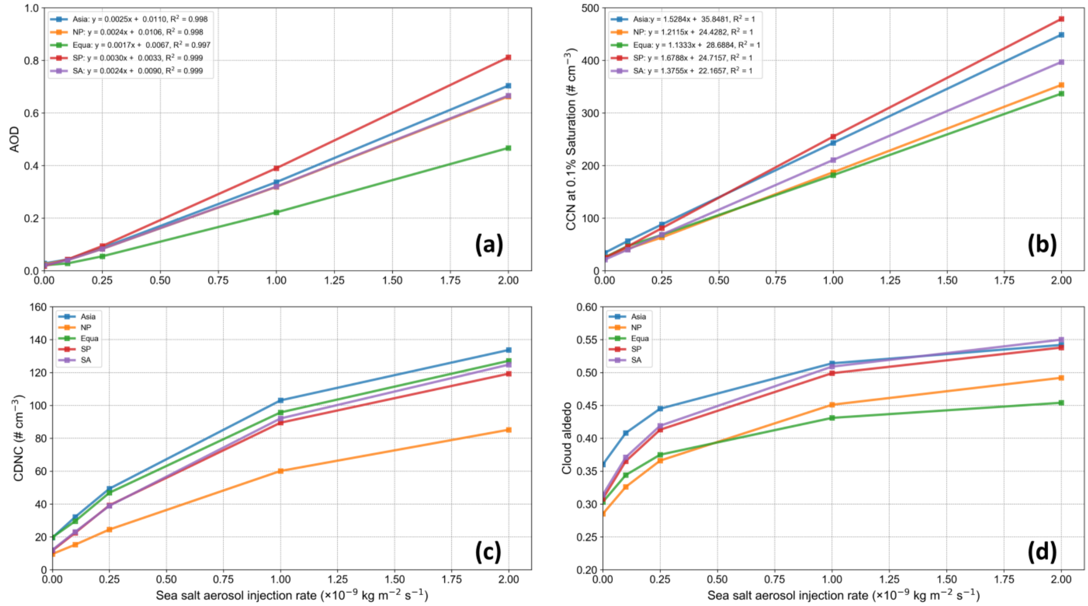

Figure 9. Relationship between changes in regional mean **(a)** AOD, **(b)** CCN, **(c)** CDNC, and **(d)** cloud albedo due to uniform injection of sea-salt aerosols across the region and the amounts of sea-salt aerosols injected. The results of the linear regression of **(a)** AOD and **(b)** CCN on the sea-salt aerosols injection amount are given at the legends.

https://doi.org/10.5194/egusphere-2024-2263
Preprint. Discussion started: 9 August 2024

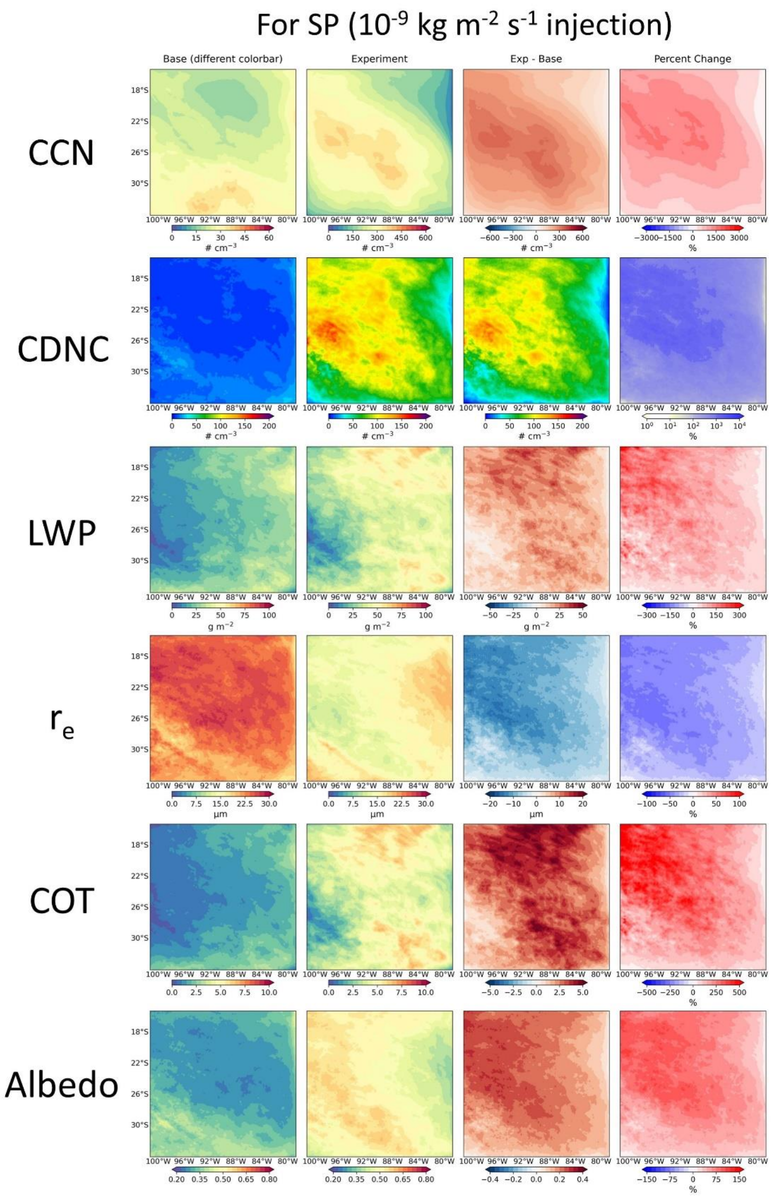

Figure 10. Spatial distribution of liquid cloud property responses after uniform injection of sea-salt aerosols with 10^{-9} kg m^{-2} s^{-1} in the SP region. Results are shown for cloud condensation nuclei (CCN, S = 0.1%, # cm^{-3}), cloud droplet number concentration (# cm^{-3}), liquid water path (LWP, g m^{-2}), cloud effective radius (r_e, μm), cloud optical thickness (COT), and cloud albedo for Base (first column), Exp (second column), Exp - Base (third column), and the percentage change in Exp - Base (fourth column), respectively.

https://doi.org/10.5194/egusphere-2024-2263
Preprint. Discussion started: 9 August 2024

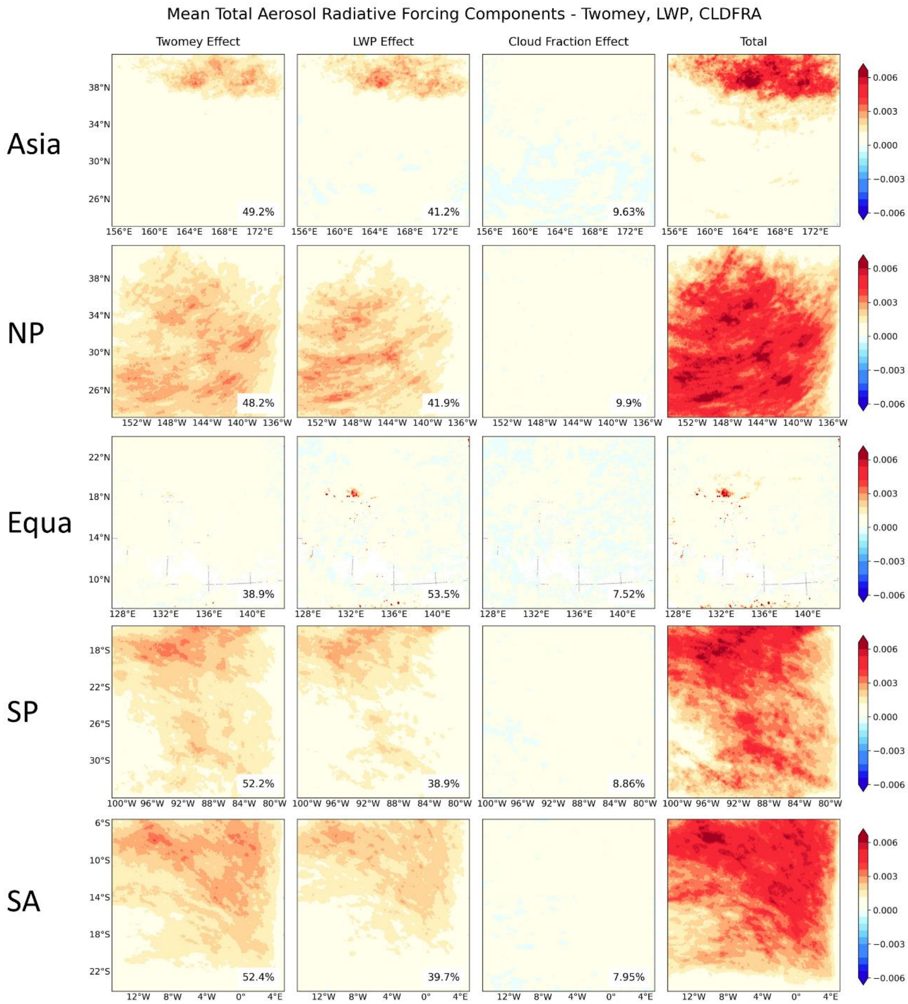

Figure 11. Spatial distribution of cloud property changes in response to SW_CLD radiation after uniform injection of sea-salt aerosols in five regions. The first column is the Twomey effect, the second column is the LWP effect, the third column is the cloud fraction effect, and the fourth column is the cloud susceptibility ($\frac{\Delta\alpha}{\Delta \ln \text{AOD}}$) to aerosol injection for the sum of the three effects. The percentage contribution of each to the total SW_CLD response over the entire region is labeled in the lower right corner.